FRICTIONAL STRENGTH OF THE CREEPING SEGMENT OF THE SAN ANDREAS FAULT

A Thesis

by

CLAYTON GAGE COBLE

Submitted to the Office of Graduate Studies of
Texas A&M University
in partial fulfillment of the requirements for the degree of

MASTER OF SCIENCE

December 2010

Major Subject: Geology

Frictional Strength of the Creeping Segment of the San Andreas Fault

FRICTIONAL STRENGTH OF THE CREEPING SEGMENT OF THE SAN ANDREAS FAULT

A Thesis

by

CLAYTON GAGE COBLE

Submitted to the Office of Graduate Studies of
Texas A&M University
in partial fulfillment of the requirements for the degree of

MASTER OF SCIENCE

Approved by:

Co-Chairs of Committee,	Frederick M. Chester
	Judith S. Chester
Committee Members,	Ahmad Ghassemi
Head of Department,	Andreas K. Kronenberg

December 2010

Major Subject: Geology

ABSTRACT

Frictional Strength of the Creeping Segment of the San Andreas Fault.

(December 2010)

Clayton Gage Coble, B.S., Sam Houston State University

Co-Chairs of Advisory Committee: Dr. Frederick M. Chester
Dr. Judith S. Chester

The San Andreas Fault (SAF) near Parkfield, CA moves by a combination of aseismic creep and micro-earthquake slip. Measurements of in situ stress orientation, stress magnitude, and heat flow are incompatible with an average shear stress on the SAF greater than approximately 20 MPa. To investigate the micro-mechanical processes responsible for the low strength and creeping behavior, gouge samples from the 3 km-deep scientific borehole near Parkfield (the San Andreas Fault Observatory at Depth, SAFOD) are sheared in a triaxial rock deformation apparatus at conditions simulating those in situ, specifically a temperature of 100°C, effective normal stress of 100 MPa, pore fluid pressure of 25 MPa, and a Na-Ca-K pore fluid chemistry. The 2 mm-thick gouge layers are sheared to 4.25 mm at shear rates of 6.0, 0.6, 0.06, and 0.006 μm/s. The mechanical data are corrected for apparatus effects and the strength of the jacketing material that isolates the sample from the confining fluid. Experiments indicate that gouge is extremely weak with a coefficient of friction of 0.14, and displays velocity and temperature strengthening behavior. The frictional behavior is consistent with the inferred in situ stress and aseismic creep observed at SAFOD. The low frictional

strength likely reflects the presence of a natural fabric characterized by microscale folia containing smectite and serpentinite.

DEDICATION

This thesis is dedicated to my mother, Elizabeth Anne Coble, and my father, Billy Glenn Coble.

ACKNOWLEDGEMENTS

I would like to thank my committee co-chairs, Dr. Frederick M. Chester and Dr. Judith S. Chester, for their guidance, patience, and support throughout the course of this research. Thank you for giving me the opportunity to take part in such scientifically and socially important research.

Thanks also go to Clayton Edward Powell for his assistance in the laboratory. Without his knowledge and help this research would not have been possible. However, I do not thank Clayton Edward Powell for blowing up the LSR. I could have done without that. I would also like to thank Hiroko Kitajima for teaching me the ways of the MVSR. Now we are leaving and taking the secrets of the MVSR with us.

Thanks also go to my friends and colleagues and the department faculty and staff for making my time at Texas A&M University a great experience.

Finally, thanks to my mother and father for their encouragement and patience.

TABLE OF CONTENTS

Page

LIST OF FIGURES

FIGURE Page

LIST OF TABLES

1. INTRODUCTION

Abundant evidence suggests that the San Andreas Fault (SAF) is a weak fault embedded in a strong crust. Evidence for a weak SAF is provided by studies of the creeping section of the fault in central California. One line of evidence is the orientation of the maximum horizontal principal compressive stress, σ_{Hmax}. Borehole breakouts and drilling-induced tensile fractures in the San Andreas Fault Observatory at Depth (SAFOD) pilot hole suggest that the σ_{Hmax} is oriented between 65° and 85° to the SAF [*Hickman and Zoback*, 2004]. At distances up to 100 km from the SAF, *Mount and Suppe* [1987] found similar stress orientations using borehole breakout measurements. Stress orientations from inversion of earthquake focal mechanisms [*Zoback et al.*, 1987; *Provost and Houston*, 2001], and thrust faults and anticlinal axes that strike subparallel to the SAF, also suggest that the σ_{Hmax} is nearly normal to the SAF [*Mount and Suppe*, 1987; *Zoback et al.*, 1987]. The orientation of σ_{Hmax} means that the shear stress resolved on the fault is small, and with the high normal stress, implies that the apparent coefficient of friction on the fault is also small. Some suggest that the coefficient of friction, μ, must be less than 0.2 [*Brune et al.*, 1969; *Mount and Suppe*, 1987; *Zoback et al.*, 1987; *Chester et al.*, 1993; *Provost and Houston*, 2001; *Chery et al.*, 2004; *Hickman and Zoback*, 2004; *Townend and Zoback*, 2004; *Williams et al.*, 2004]. Another line of evidence for a weak SAF is the lack of a local increase in heat flow along the fault

---

This thesis follows the style of *Journal of Geophysical Research.*

[*Brune et al.*, 1969; *Lachenbruch and Sass*, 1980; *Williams et al.*, 2004]. An increase in heat flow caused by frictional heating would be expected if the fault were strong, i.e., the coefficient of friction is greater than the 0.5 typical of most rocks (e.g., *Byerlee*, 1978). Based on the orientation of the σ_{Hmax} and no evidence for increased heat flow two conclusions can be drawn: 1) The magnitude of shear stress causing the SAF to creep must be small, and 2) for slip to occur at a small magnitude of shear stress, the fault must be weak in a relative or absolute sense.

Several hypotheses have been presented to explain the weakness of the SAF [*Rutter*, 1983; *Sibson*, 1992; *Chester et al.*, 1993; *Rice*, 2006; *Schleicher et al.*, 2006; *Moore and Lockner*, 2008]. These include hypotheses that explain fault weakness during seismic slip (from dynamic weakening mechanisms), and those that explain weakness under quasi static conditions as occurs during aseismic creep. Near Parkfield, CA, where SAF displacement occurs through a combination of aseismic creep and repeating micro-earthquakes, dynamic weakening mechanisms cannot explain the apparent weakness [*Moore and Lockner*, 2008]. The favored hypotheses for fault weakening at aseismic creep rates include: 1) intrinsically weak minerals, e.g., smectite and talc, are present in the fault that allow frictional slip at a low resolved shear stress [*Logan and Rauenzahn*, 1987; *Reinen et al.*, 1991; 1994; *Saffer and Marone*, 2003; *Moore and Lockner*, 2004; 2008], 2) elevated pore fluid pressures are maintained within the fault core, which lowers the effective normal stess on the fault and allows slip at a low resolved shear stress [*Byerlee and Brace*, 1972; *Lachenbruch*, 1980; *Rice*, 1992; *Sibson*, 1992; *Chester et al.*, 1993], 3) pressure-independent deformation mechanisms (e.g., dissolution-aided

slip and dislocation glide in phyllosilicates) dominate the slip behavior at low strain rates, allowing for aseismic creep and distributed shear under low levels of shear stress [*Rutter and Mainprice*, 1978; *Rutter*, 1983; *Chester et al.*, 1993; *Hickman and Evans*, 1995; *Wintsch et al.*, 1995; *Bos et al.*, 2000; *Morrow et al.*, 2000; *Moore and Lockner*, 2004], and 4) the presence of a natural fabric characterized by a preferred orientation of weak minerals (e.g., mica) along folia allowing for sliding at low coefficients of friction [*Shea and Kronenberg*, 1992; *Wintsch et al.*, 1995; *Carpenter et al.*, 2009; *Collettini et al.*, 2009; *Niemeijer et al.*, 2010; *Smith and Faulkner*, 2010].

While small magnitude earthquakes occur within the creeping section of the SAF, no large magnitude earthquakes have been observed [*Tocher*, 1960; *Allen*, 1968; *Brown and Wallace*, 1968]. This is evidence that the aseismic creeping section of the SAF is velocity-strengthening (frictional strength increases as slip velocity increases), a behavior that causes only stable slip (*Marone and Scholz*, 1988; *Scholz*, 1998). The rate-dependence of frictional strength is a material property, and certain minerals have been found to be rate strengthening, e.g., serpentine, talc, smectite, and illite (*Moore et al*., 1997; *Saffer and Marone*, 2003; *Moore and Lockner*, 2008).

To explore fault weakening mechanisms experiments have been conducted on exhumed fault rocks [*Chester and Logan*, 1986; *Rutter et al.*, 1986; *Numelin et al.*, 2007; *Collettini et al.*, 2009; *Smith and Faulkner*, 2010], and on artificial gouge containing representative minerals found in natural faults [*Logan and Rauenzahn*, 1987; *Reinen et al.*, 1991; *Chester*, 1994; *Beeler et al.*, 1996; *Morrow et al.*, 2000; *Saffer and Marone*, 2003; *Moore and Lockner*, 2004; *Escartin et al.*, 2008; *Moore and Lockner*, 2008;

Carpenter et al., 2009; *Ikari et al.*, 2009; *Niemeijer et al.*, 2010; *Tembe et al.*, 2010]. Few experimental studies of friction, however, have been conducted on fault rocks taken from an active fault at seismogenic depth [*Tembe et al.*, 2006; *Morrow et al.*, 2007; *Carpenter et al.*, 2009; *Tembe et al.*, 2009; *Kitajima et al.*, Frictional behavior of SAFOD fault rocks sheared at seismic slip rates, manuscript in preperation, 2010, hereinafter referred to as Kitajima et al., manuscript in preperation, 2010]. Still fewer studies have explored the friction behavior of these rocks at in situ conditions [*Tembe et al.*, 2009]. The San Andreas Fault Observatory at Depth (Figure 1) has provided the opportunity to study materials taken from the actively creeping, aseismic segment of the SAF. The SAFOD borehole intersects two actively creeping traces of the SAF at approximately 3 km depth. These fault traces are referred to as the Southwest Deforming Zone (SDZ) at 3192 m measured depth (MD) and the Central Deforming Zone (CDZ) at 3302 m MD [*Zoback et al*., 2010]. The measured depths correspond to true vertical depths of 2620 and 2675 m, respectively. The creeping zones are composed of dark grayish-black, ultrafine-grain, foliated fault gouge that contains clasts of serpentinite, siltstone, and fine-grained sandstone.

The purpose of this study is to determine the frictional strength and deformation mechanisms that are active within the aseismic creeping section of the SAF at SAFOD. By simulating conditions at seismogenic depths, retaining in part the natural gouge fabric, and conducting experiments at low strain rates, I will test two hypotheses: 1) The gouge taken from the active creeping section of the SAF at 3 km depth is strongly rate-

a.

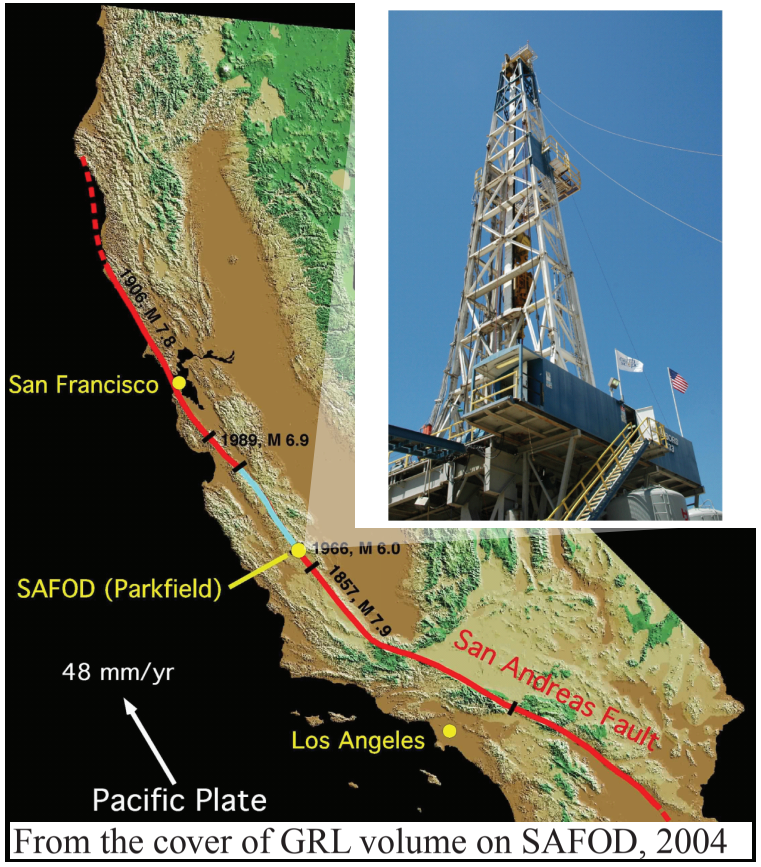

b.

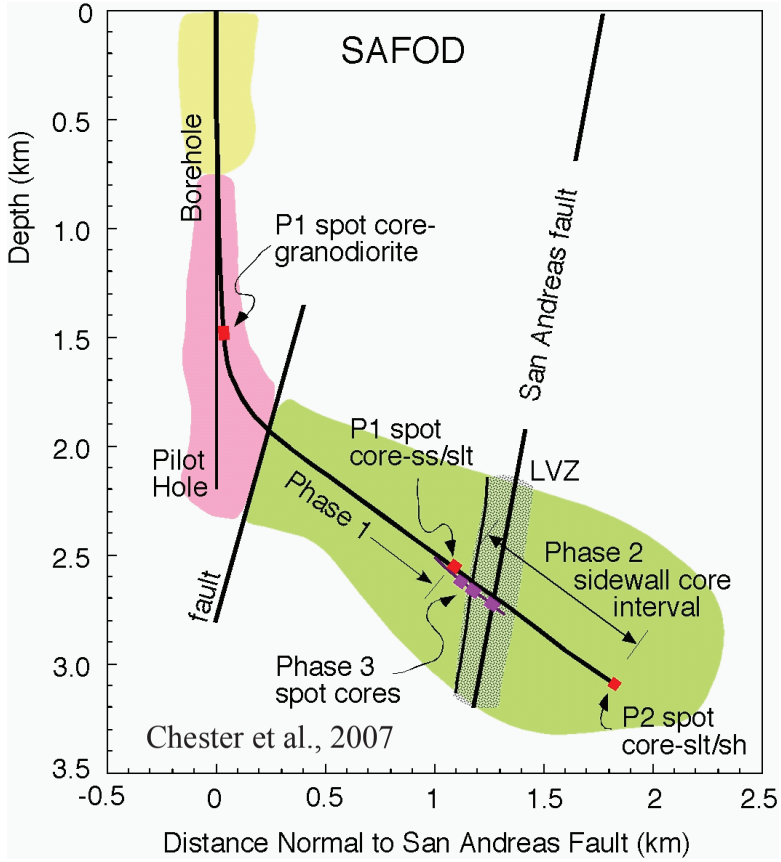

Figure 1. (a) The SAFOD site is located along the aseismic creeping section of the SAF (light blue) in central California near the town of Parkfield. The northern and southern sections of the SAF (red) are locked and slip along these sections of the fault occurs by large magnitude earthquakes. (b) Initial drilling of the SAFOD borehole took place on the west side of the fault. The borehole was then deviated and crossed the SAF at 2.7 km true vertical depth. The SAF gouge used in this study was taken from the Phase 3 spot cores. [(a) is from Hickman et al., 2004 and (b) is from Chester et al., 2007]

strengthening, 2) When sheared at low strain rates representative of the creeping zones of the SAF, the gouge will be weak.

To test these hypotheses, and thus their applicability to understanding long-term fault weakening along the creeping section of the SAF, I will conduct friction experiments on analog fault materials and on natural fault gouge from the SAF collected at SAFOD (hereafter referred to as SAFOD gouge). The friction experiments will be run at conditions simulating the natural environment of the SAF intersected by the borehole. Gouge from the CDZ at 3 km depth at SAFOD will be sheared at 100°C, an effective normal stress of 100 MPa, a pore fluid pressure of 25 MPa, pore fluid chemistry similar to the formation fluid at SAFOD, and shear slip rates of 6.0, 0.6, 0.06, and 0.006 μm/s.

2. METHOD

2.1. Triaxial Shear Experiments

Triaxial shear experiments are conducted by placing a thin layer of gouge between a sawcut, in a cylindrical forcing block. The sawcut is oriented at 35° to the shortening direction and long axis of the cylinder (Figure 2). All experiments are conducted in a gear-driven, variable strain-rate, triaxial rock deformation apparatus using silicone fluid as the confining medium [*Heard*, 1963; *Chester*, 1988; 1989]. The apparatus incorporates an internal force gauge for sensitive force measurements, an external furnace for stable temperatures with small temperature gradients in the sample, an independently controlled pore fluid pressure system incorporating a volumeter used to measure pore fluid volume changes, and corrosion-resistant stainless steel and inconel plumbing to minimize reactions between the apparatus and pore fluids.

All experiments are conducted at constant effective normal stress by manually maintaining a constant pore fluid pressure and adjusting the confining pressure during shortening. Real-time monitoring of experimental conditions is used to calculate the effective normal stress, which allows for the confining pressure to be adjusted appropriately. The calculation of effective normal stress also takes into account the strength of the sealing jacket that isolates the sample from the confining fluid. Parameters recorded during the experiment are elapsed time, confining pressure (accuracy of 0.07 MPa), pore fluid pressure, P_p (with an error of less than 0.02 MPa),

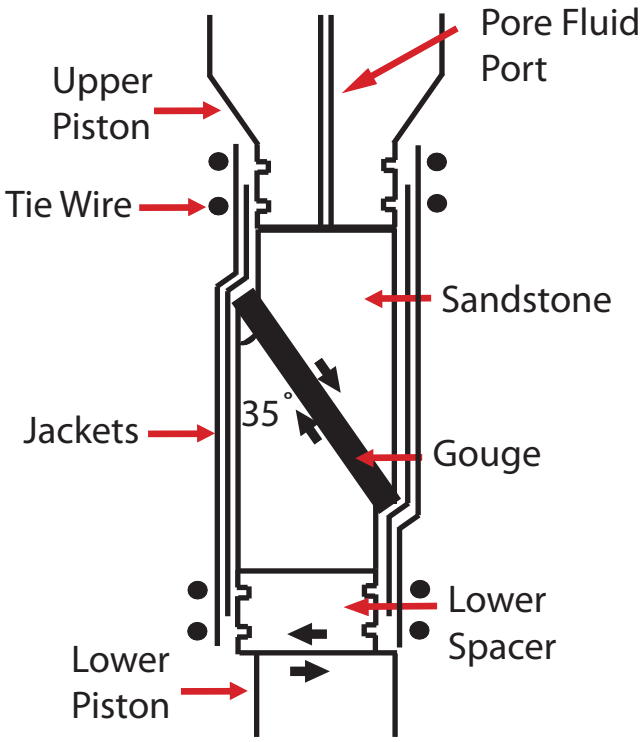

Figure 2. Sample assembly and jacketing configuration used for the SAFOD Inter-laboratory Comparison Study and for the SAFOD Gouge Study. Note that for the SAFOD Inter-laboratory Comparison Study an additional inner jacket is used that is not pictured.

displaced pore fluid pressure volume (accurate to 0.02 cc), differential axial force (accurate to 0.2 MPa), axial displacement (accurate to 5×10^{-3} mm), and temperature (with an error of less than 1°C).

A Coconino Sandstone cylinder measuring 19.05 mm in diameter is used as the forcing block. The sandstone porosity (~13.7 – 14.8%) and high permeability (~4.23 x 10^{-15} – 2.16 x 10^{-14}) facilitate transmission of the pore fluid to the gouge layer and maintenance of the desired P_p. The 35° pre-cut surfaces are wet-sanded with 220 grit silicon carbide sand paper to produce uniform and repeatable roughness.

To isolate the sandstone and gouge from the confining fluid, jackets are placed around the sample. The room-T tests employ three heat-shrink polyolefin jackets to isolate the sample from the confining fluid. The inner jacket encases the sample, the intermediate jacket covers the sample, part of the upper piston, and part of the lower spacer, and the outer jacket covers the sample and is attached to the upper piston and lower spacer with a tie wire (Figure 2).

For the experiments performed at relatively high temperatures an inner silver foil is placed around the sample followed by a single, outer Teflon jacket to seal the sample. The forcing blocks are wrapped in silver foil, followed by a Teflon jacket that is attached to the lower spacer and upper piston by tie wires. During long term SAF gouge experiments the silver foil reduces the diffusion of pore fluid through the Teflon jacket and out of the sample.

The inner jacket is cut at an angle similar to the lower pre-cut cylinder to facilitate sample assembly and production of a uniform thickness of gouge before

placing the sandstone blocks together and applying the intermediate jacket. Samples are saturated in a vacuum chamber overnight with either distilled water or brine before applying the outer jacket and sealing the assembly with tie-wires.

2.2. Experiments for SAFOD Inter-laboratory Comparison Study

The analog gouge materials used in the SAFOD Inter-laboratory Comparison Study were prepared at the Rock Mechanics Laboratory at The Pennsylvania State University by Chris Marone and Brent Carpenter. The analog gouges are composed of 1) quartz, 2) a 50/50 mixture of quartz and montmorillonite, 3) Westerly Granite, 4) talc, and 5) cuttings taken during SAFOD Phase III drilling from a shale unit intersected in Hole E at a depth of 10,366 to 10,430 ft. All gouge materials were first disaggregated to < 190 μm diameter particles and then shipped to the participating laboratories. The analog gouge experiments used a 1 mm layer of simulated fault gouge. The friction experiments were conducted at constant effective normal stresses of 10 MPa and 100 MPa, a P_p of 5 MPa, and room temperature (Table 1). Distilled water was used for the pore fluid. A shear displacement of 4.25 mm was imposed at a rate of 0.6 μm/s. As per requirements of the Inter-lab comparison study, the experiments employed slide-hold-slide tests, with holds at 2.25 mm, 2.50 mm, 2.75 mm, 3.00 mm, and 3.25 mm, for 10 s, 30 s, 100 s, 300 s, and 1000 s, respectively. Velocity steps were not carried out because the apparatus does not permit stepping at high slip rates.

2.3. Experiments on SAFOD Gouge

The SAFOD gouge used in this study was taken from core samples obtained from the CDZ of the SAF, and is from Hole G, Core Run 4, Section 4 at 9 cm from the

Table 1. Matrix of shear experiments on gouge layers to determine coefficient of friction.

Gouge Type	Exp. #	w (mm)	T (C)	σ_n^e (MPa)	P_p (MPa)	Pore Fluid	Test Type	Shear displ. rate (μm/s)	d (mm)
Quartz	IC-Q-100	1	Room	100	5	D.W.	SHS	0.6	3.90
Quartz	IC-Q-10	1	Room	10	5	D.W.	SHS	0.6	4.25
Quartz/Mont.	IC-QM-100	1	Room	100	5	D.W.	SHS	0.6	4.10
Quartz/Mont.	IC-QM-10	1	Room	10	5	D.W.	SHS	0.6	4.25
Westerly Granite	IC-G-100	1	Room	100	5	D.W.	SHS	0.6	3.90
Westerly Granite	IC-G-10	1	Room	10	5	D.W.	SHS	0.6	4.25
Talc	IC-T-100	1	Room	100	5	D.W.	SHS	0.6	4.10
Talc	IC-T-10	1	Room	10	5	D.W.	SHS	0.6	4.25
SAFOD Cuttings	IC-C-100	1	Room	100	5	D.W.	SHS	0.6	3.90
SAFOD Cuttings	IC-C-10	1	Room	10	5	D.W.	SHS	0.6	4.25
SAFOD Gouge	SG-9	1	Room	100	5	D.W.	SHS	0.6	4.25
SAFOD Gouge	SG-10	1	Room	10	5	D.W.	SHS	0.6	4.25
SAFOD Gouge	SG-5	2	100	100	25	Brine	σ_n^e only	N/A	0.0
SAFOD Gouge	SG-3	2	100	100	N/A	Dry	SHS	0.6	4.25
SAFOD Gouge	SG-1	2	100	100	25	Brine	SHS	0.6	4.25
SAFOD Gouge	SG-2	2	100	100	25	Brine	SHS	0.6	4.25

Table 1 continued.

Gouge Type	Exp. #	w (mm)	T (C)	σ_n^e (MPa)	P_p (MPa)	Pore Fluid	Test Type	Shear displ. rate (μm/s)	d (mm)
SAFOD Gouge	SG-4	2	100	100	25	Brine	SHS	0.006	3.90
SAFOD Gouge	SG-6	2	100	100	25	Brine	VS	0.6, 0.06, 0.006	4.25
SAFOD Gouge	SG-7	2	100, 80, 120	100	25	Brine	TS, VS	0.6, 0.06, 0.006	4.25
SAFOD Gouge	SG-8	2	100	100	25	Brine	VS	6.0, 0.6, 0.06	4.25

w, Gouge Thickness; T, Temperature; σ_n^e, Effective Normal Stress; P_p, Pore Pressure; d, Shear Displacement; SHS, Slide-hold-slide; VS, Velocity Stepping; TS, Temperature Stepping; D.W., Distilled Water; N/A, Not Applicable.

top of the section. The gouge was gently disaggregated to a diameter of 844 μm; the large particle size is used to preserve the natural fabric and porphyroclasts within the gouge. A 2 mm thick gouge layer, corresponding to a mass of 2.65 g, is placed between the Coconino Sandstone forcing blocks.

The pore fluid brine matches the concentration of the primary ionic components of the formation fluid recovered from the SAFOD borehole at a measured depth of 3594 m. The concentration of the primary ionic components of the formation fluid is 15.7 g/L of Cl, 5.72 g/L of Na, 3.62 g/L Ca, and 0.22 g/L of K [Y. Kharaka and J. Thordsen, personal communication, 2007]. The pore fluid was created by adding 4.25 g of KCl, 14.74 g of NaCl, and 10.02 g of $CaCl_2$ per 1 L of distilled water.

Experiments are performed at a constant effective normal stress of 100 MPa, P_p of 25 MPa (except for the dry sample), and at a temperature of 100°C (with the exception of the temperature stepping experiment) to best simulate the conditions at 3 km depth in the fault zone (Table 1). The sample is allowed to equilibrate at temperature and pressure for 24 hours prior to sliding. Two experiments conducted on the SAFOD gouge are performed at the same conditions as the SAFOD Inter-laboratory Comparison Study experiments.

2.4. Jacket Strength Determination

To accurately measure the coefficient of friction, particularly for very weak gouge, the strength of the jackets must be determined as a function of effective pressure and displacement. Therefore, dedicated experiments are conducted to determine jacket strength for room-T and high-T tests. The strength of the room-T and high-T jackets is

determined in dedicated experiments using the same sample and jacketing configuration as the gouge experiments except 1) the cut cylinders are steel, 2) the inclined surface is lubricated with MoS_2 at room-T, and silicone fluid at high-T, to reduce sliding friction, and 3) pore fluids are not used. The steel cylinder is 18.542 mm in diameter, and experiments are conducted at a constant confining pressure (Table 2).

Jacket strength is determined following the analysis of mechanical data outlined by *Chester* [1994]. The effective normal stress, σ_n^e, and shear stress, τ, across the pre-cut surface are given by

$$\sigma_n^e = (P_c - P_p) + [(\Delta F_t - \Delta F_j)\sin^2\theta + \mu_{ls}\Delta F_t\cos\theta\sin\theta] / A_{ls} \quad (1a)$$

$$\tau = [(\Delta F_t - \Delta F_j)\cos\theta\sin\theta - \mu_{ls}\Delta F_t\sin^2\theta] / A_{ls} \quad (1b)$$

where P_c is the confining pressure, P_p is the pore fluid pressure, θ is the angle between the pre-cut surface and the maximum principal stress (35°), ΔF_t is the differential force, ΔF_j is the differential force supported by the jackets, μ_{ls} is the coefficient of friction of the interface between the lower piston and lower spacer, and A_{ls} is the cross-sectional area of the interface between the lower piston and lower spacer. From $\tau = \mu\sigma_n^e$, where μ is the coefficient of friction of the 35° sliding interface, equations (1a) and (1b) may be substituted to derive a single expression relating the three unknowns, μ, ΔF_j, and μ_{ls}.

$$\mu = \frac{\tau}{\sigma_n^e} = \frac{[(\Delta F_t - \Delta F_j)\cos\theta\sin\theta - \mu_{ls}\Delta F_t\sin^2\theta]}{(P_c - P_p) + [(\Delta F_t - \Delta F_j)\sin^2\theta + \mu_{ls}\Delta F_t\cos\theta\sin\theta]} \quad (2)$$

Using (2), the best fit values of μ and μ_{ls} are determined from the suite of jacket strength tests, and ΔF_j is determined as a function of effective pressure and displacement.

Table 2. Matrix of experiments to determine jacket strength.

Experiment Number	Jacket Type	Pc (MPa)	T (C)	Shear displ. rate (μm/s)	Shear Displ. (mm)
3P-15-1	3 Polyolefin	15	Room	0.6	4.0
3P-40-1	3 Polyolefin	40	Room	0.6	4.0
3P-75-1	3 Polyolefin	75	Room	0.6	4.0
3P-75-2	3 Polyolefin	75	Room	0.6	4.0
3P-100-1	3 Polyolefin	100	Room	0.6	4.0
ST-80-1	Silver and Teflon	80, 60	100	0.6	4.0
ST-50-1	Silver and Teflon	50, 70	100	0.6	4.0
ST-80-2	Silver and Teflon	80	100	0.6	4.0

2.4.1 Room-T Jacket Strength

The strength of the jacketed sample assembly is dependent on both effective confining pressure and the magnitude of displacement over the range of effective confining pressures tested (Figure 3). The analysis used to determine the room-T jacket strength included determining the coefficient of friction of the two sliding interfaces. Initial analysis of the results using (2) indicates the coefficient of friction of the lubricated sliding surfaces is a function of P_e. Accordingly, the coefficient of friction of the two sliding interfaces is determined by analyzing pairs of experiments independently, i.e., 100 and 75 MPa, 75 and 40 MPa, and 40 and 15 MPa (Figure 3). Through iteration, the best fit coefficients of friction are determined, assuming that the jacket strength is the same in each pair of tests. The analysis indicates that the coefficient of friction of MoS_2 is relatively high at low effective confining pressures, and decreases monotonically with an increase in effective confining pressure (Figure 3). Interpolating between the determined values of the coefficient of friction of the sliding surface, the jacket strength is determined for each calibration test (Figure 4). Results of the analysis indicates that jacket strength increases with effective confining pressure at pressures less than 40 MPa, and is relatively constant at pressures greater than 40 MPa. Interpolating sliding surface friction and jacketed assembly strength between P_e of 15 MPa and 0 MPa (where jacketed assembly strength is nominal) suggests jacket strength increases linearly with P_e up to a P_e of 15 MPa. The increase in jacket strength with P_e is thought to reflect the increased bonding between jackets and sawcut blocks from the increase in P_e. At each effective confining pressure tested the jackets exhibit work-hardening behavior

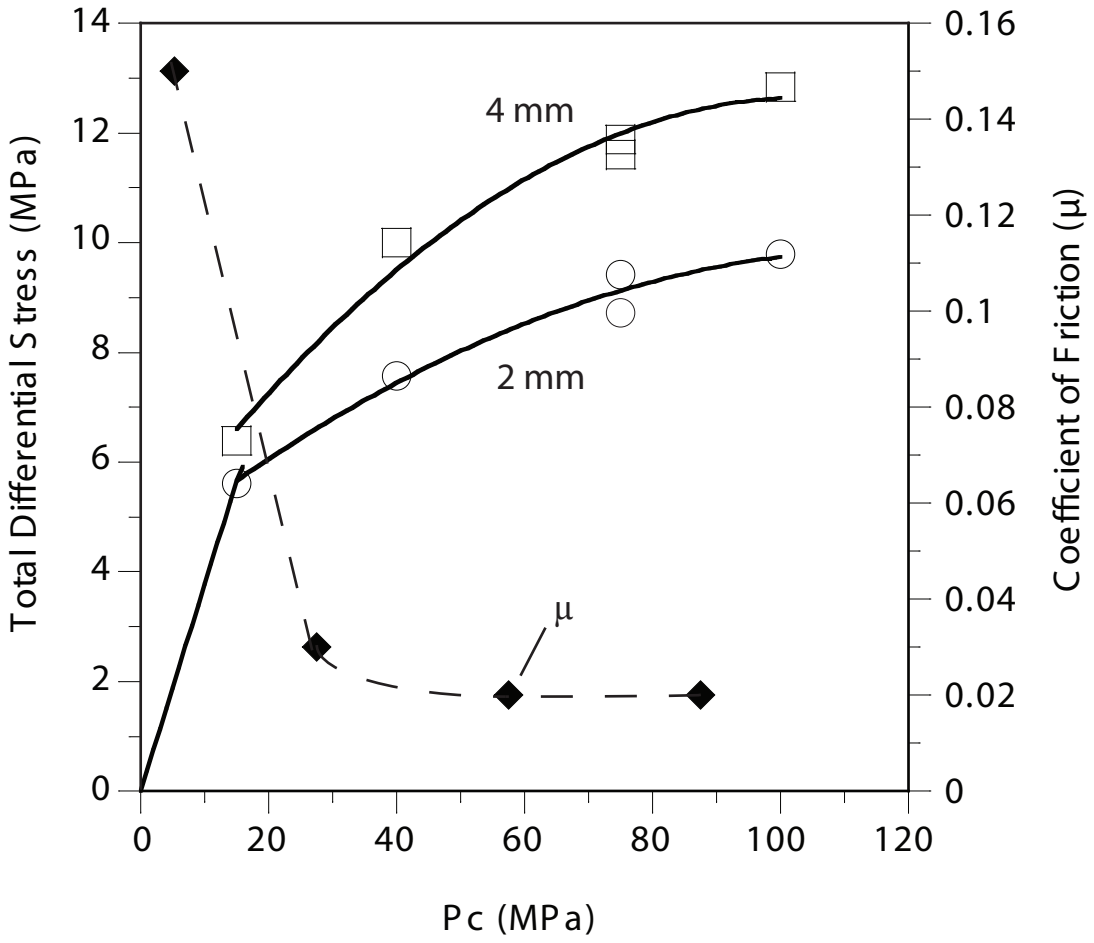

Figure 3. Total strength of the jacketed sample used for jacket tests and the coefficient of friction of the MoS_2 lubricated inclined surface versus effective confining pressure. Total strength measurements are made at shear displacements of 2 (open circles) and 4 mm (open squares). The strength data is used to determine the coefficient of friction of the sliding surfaces (molycote friction shown by solid diamonds) using (2) described in the text.

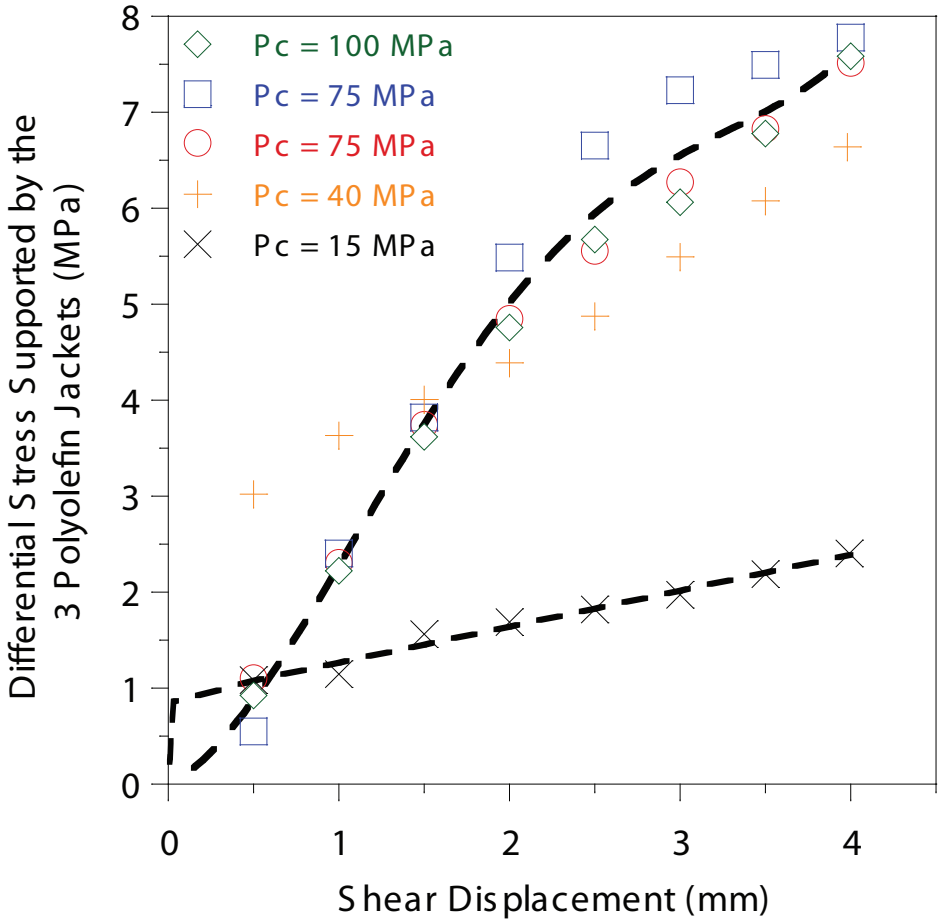

Figure 4. Plot of the differential stress supported by the three polyolefin jackets as a function of shear displacement for each effective confining pressure tested. Jacket strength was calculated at shear displacement intervals of 0.5 mm. Two curves are distinguished for relatively high (100, 75, and 40 MPa) and low confining pressures (15 MPa). At relatively high effective confining pressures the jacket is stronger and the work-hardening rate is more rapid than at relatively low effective confining pressures. Equation 3 (relatively high effective confining pressure) and equations 4 and 5 (relatively low effective confining pressure) are used to calculate the jacket strength.

(Figure 4). At relatively high effective confining pressures appropriate for friction tests on gouge at an effective normal stress of 100 MPa, jacket strength solely depends on displacement and is adequately described by a fourth-order polynomial

$$\Delta\sigma_j = 0.10d^4 - 0.89d^3 + 2.18d^2 + 0.88d \quad (3)$$

where $\Delta\sigma_j$ is the differential stress supported by the jackets in MPa and d is the shear displacement in mm. At relatively low confining pressures appropriate for friction test on gouge at an effective normal stress of 10 MPa, jacket strength is described with a bi-linear relationship representing an elastic-plastic response where the plastic strength varies with pressure and with displacement (Figure 4), consistent with the P_e-dependence shown in Figure 3. For small displacements

$$\Delta\sigma_j = (28.75*d) \quad (4)$$

and for large displacements

$$\Delta\sigma_j = [(0.38*d) + 0.89] * (P_e/15) \quad (5)$$

where P_e is the effective confining pressure (P_c - P_P) in MPa. The effective confining pressure term is normalized by the confining pressure used during the relatively low pressure jacket strength test (15 MPa) to represent the dependence of jacket strength on effective pressure.

2.4.2 High-T Jacket Strength

During the experiments in which effective confining pressure is changed, the jackets are slightly stronger at a $P_e$of 80 and 60 MPa compared to the $P_e$of 50 and 70

MPa (Figure 5). The variation in strength caused by changes in confining pressure are less than the magnitude of sample-to-sample variation, thus it is assumed that jacket strength is independent of effective pressure. Therefore, the strength of the silver and Teflon jackets are solely dependent on shear displacement. A bilinear relationship is needed to describe the strength of the jackets at small and large displacements. For small displacements

$$\Delta\sigma_j = 71.35d \tag{6}$$

and for large displacements

$$\Delta\sigma_j = 1.41d + 2.05 \tag{7}$$

where $\Delta\sigma_j$ is the differential stress supported by the silver and Teflon jackets in MPa and d is the shear displacement in mm.

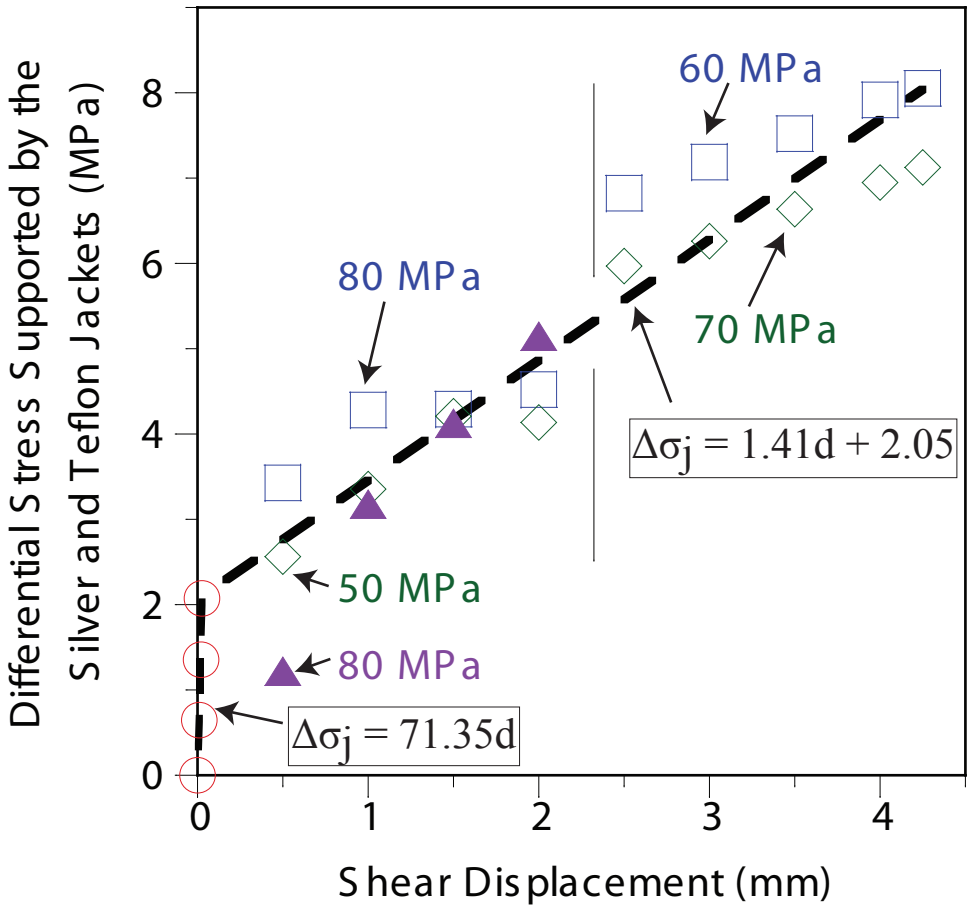

Figure 5. Plot of the differential stress supported by the silver foil and Teflon jacket at 100°C as a function of shear displacement for effective confining pressures of 50, 60, 70, and 80 MPa. Jacket strength was calculated at shear displacement intervals of 0.5 mm. The jacket strength varies little with effective confining pressure. The jackets work-harden and are best described by two equations for small displacements (6) and large displacements (7).

3. RESULTS

3.1. SAFOD Inter-Laboratory Comparison Study

The five analog gouge materials display a wide range of frictional strengths (Figure 6). Quartz, Westerly Granite, and the SAFOD Cuttings have typical coefficients of friction for rocks [Byerlee, 1978], while the talc and quartz/montmorillonite 50/50 mixture is weaker than normal. Generally, the coefficient of friction at high σ_n^e ranges from 8% to 27% less than at low σ_n^e. Talc is the weakest material at each normal stress ($\mu = 0.2$). The SAFOD cuttings are the strongest material at low σ_n^e, 10 MPa, ($\mu = 0.7$), and quartz and the SAFOD cuttings are the strongest material at high σ_n^e, 100 MPa, ($\mu = 0.6$). The analog gouge materials with high coefficients of friction, such as quartz, Westerly Granite, and the SAFOD Cuttings, tend to work-harden. Gouge with a low coefficient of friction, such as talc and the quartz/montmorillonite mixture, displays frictional behavior closer to steady state with small hardening or softening.

Our results from the SAFOD Inter-laboratory Comparison Study compare well with those of the other participating groups. At 10 MPa effective normal stress, the coefficient of friction values determined in this study are between 5 and 36% higher than the coefficient of friction values calculated by averaging the five participating groups (Table 3 and Figure 7). The quartz/montmorillonite 50/50 mixture has the largest range in coefficient of friction values, 0.13, when comparing the average of the five groups to this study. Comparing data from each lab, friction values for gouge with a higher

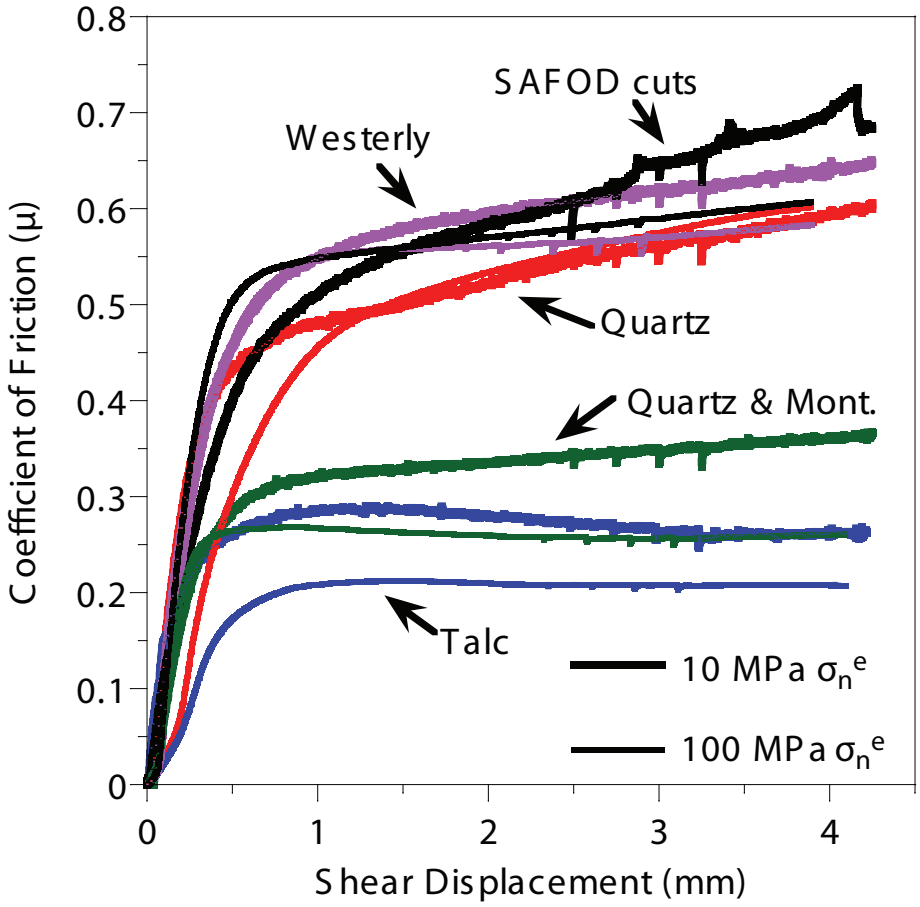

Figure 6. SAFOD Inter-laboratory Comparison Study experiments. A plot of the coefficient of friction, μ, versus shear displacement for 10 experiments conducted at room temperature. Experiments conducted at a constant effective normal stress (σ_n^e) of 100 MPa are plotted with thin lines, and 10 MPa are plotted with thick lines. Five holds (slide-hold-slide tests) are conducted during each experiment for 10, 30, 100, 300, and 1000 s, and are characterized by reductions in μ during each hold.

Table 3. Results for experiments conducted at an effective normal stress of 10 MPa from the five groups participating in the SAFOD Inter-laboratory Comparison Study.

Gouge Compostion	Penn State University	USGS	Utrecht University	Padua University	University of Bremen	Average	**This Study**
Quartz	0.66	0.72	0.39	-	0.46	0.56	**0.59**
Quartz/ Mont.	0.32	0.26	0.12	-	0.20	0.23	**0.36**
Talc	0.25	0.26	0.08	0.27	0.15	0.20	**0.26**
Westerly Granite	0.66	0.80	0.42	-	0.50	0.60	**0.63**
SAFOD Cuttings	0.66	0.74	0.43	0.63	0.48	0.59	**0.69**

Coefficient of friction measurements are taken at 90% of the final displacement for each experiment. Experiments using an effective normal stresses of 11 MPa are included in the Utrecht University measurements. Experiments using an effective normal stresses of 3 MPa are included in the Padua University measurements.
Researchers include: Penn State University, Carpenter, Marone, and Saffer; USGS, Lockner and Morrow; Utrecht University, Spiers, Peach, and de Bresser; Padua University, Ferri, Di Toro, De Rossi, and Quaresimin; University of Bremen, Kopf.

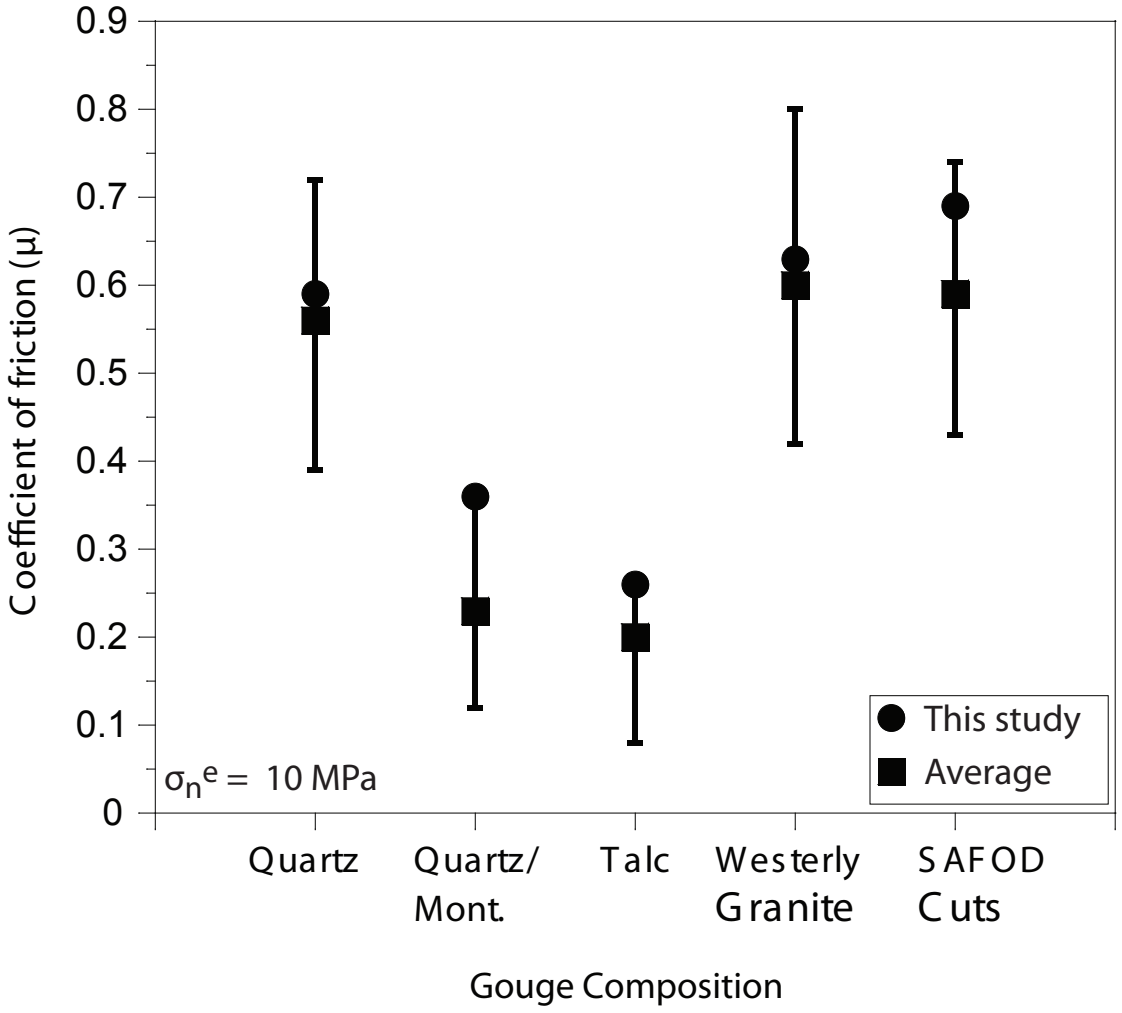

Figure 7. The coefficient of friction for the five analog gouge materials determined by the five participating groups compared to this study (filled circle). Experiments were performed at a constant effective normal stress of 10 MPa. The average coefficient of friction calculated for the five participating groups for each gouge is represented by a filled square. The error bars represent the range of the coefficient of friction values for each gouge.

average frictional strength show more scatter. For instance, the coefficient of friction for Westerly Granite ranged from 0.42 to 0.80, a difference of 0.38. In the 100 MPa effective normal stress experiments, coefficient of friction values determined in this study are 9 to 28% lower than the average coefficient of friction values for the two groups (Table 4 and Figure 8). For Westerly Granite, the average coefficient of friction, 0.69, and the coefficient of friction determined in this study, 0.58, is the largest difference in frictional strength at 100 MPa.

Various apparatus, including direct shear, rotary shear, as well as triaxial shear, were used by the participating groups to perform experiments in the SAFOD Inter-laboratory Comparison Study. Each apparatus and jacketing assembly requires individual corrections. The fact that our results compare well with those of others lead us to believe that our jacket corrections are appropriate, and that the coefficient of friction values determined are accurate.

3.2. SAFOD Gouge Study

3.2.1. Frictional Strength of the SAFOD Gouge

The strength of the SAFOD gouge is most comparable to the talc and the quartz/montmorillonite 50/50 mixture from the Inter-laboratory Comparison Study. At both 10 and 100 MPa effective normal stress the SAFOD gouge is the weakest gouge material tested (Figure 9a). At higher effective normal stresses the coefficient of friction values for each gouge material are reduced, relative to the lower effective normal stress experiments, by 14% for SAFOD gouge, 20% for talc, and 27% for the

Table 4. Results for experiments conducted at an effective normal stress of 100 MPa from two groups participating in the SAFOD Inter-laboratory Comparison Study.

Gouge Compostion	USGS	Utrecht University	Average	**This Study**
Quartz	0.72	0.60	0.66	**0.59**
Quartz/ Mont.	0.28	0.44	0.36	**0.26**
Talc	0.24	0.21	0.23	**0.21**
Westerly Granite	0.70	0.68	0.69	**0.58**
SAFOD Cuttings	0.66	0.68	0.67	**0.60**

Coefficient of friction measurements are taken at 90% of the final displacement for each experiment. Experiments using an effective normal stresses of 97, 99, and 100 MPa are included in the Utrecht University measurements.
Researchers include: USGS, Lockner and Morrow; Utrecht University, Spiers, Peach, and de Bresser.

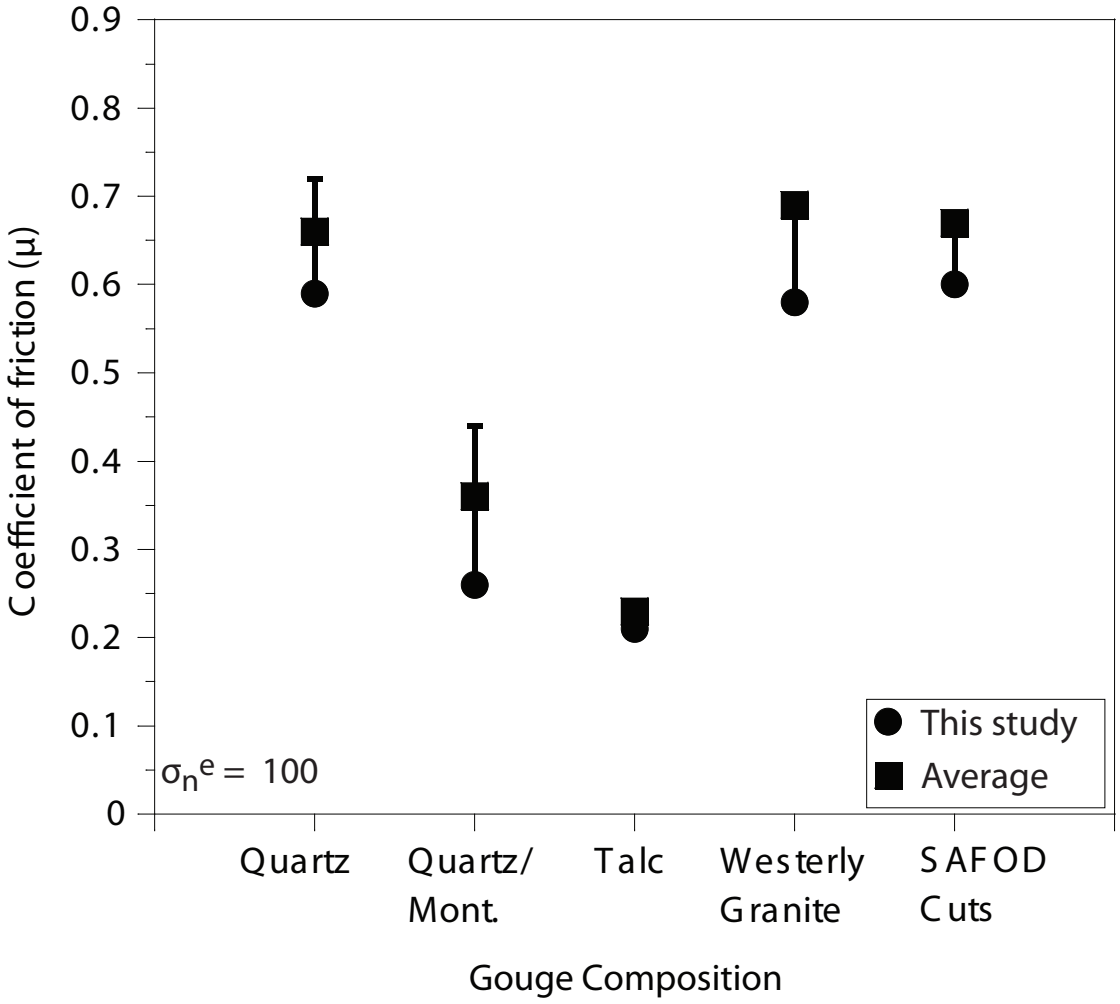

Figure 8. The coefficient of friction for the five analog gouge materials determined by the five participating groups compared to this study (filled circle). Experiments were performed at a constant effective normal stress of 100 MPa. The average coefficient of friction calculated for the two participating groups for each gouge is represented by a filled square. The error bars represent the range of the coefficient of friction values for each gouge.

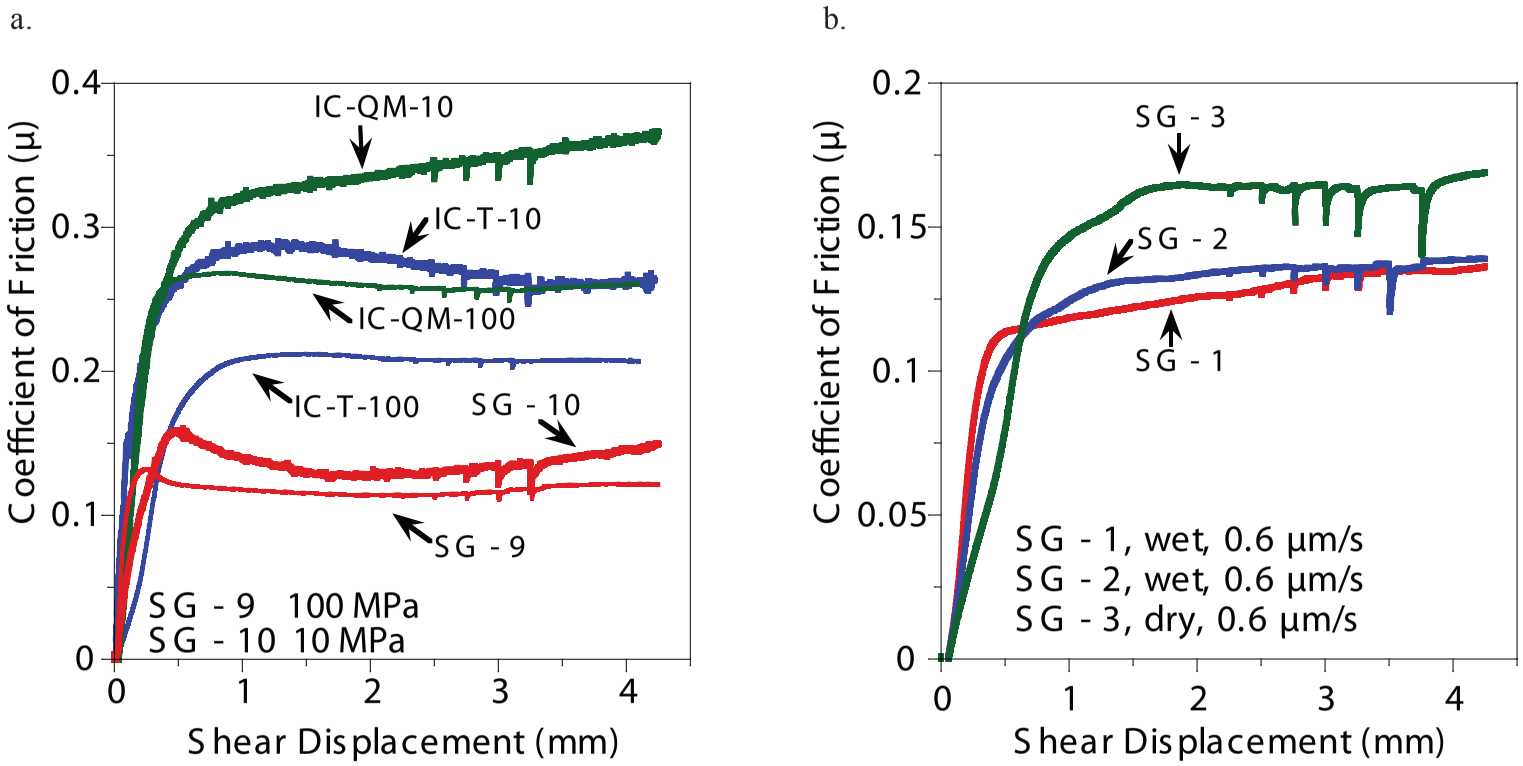

Figure 9. Friction versus shear displacement plot of (a) SAFOD Gouge, talc, and quartz/ montmorillonite 50/50 mixture and (b) wet and dry SAFOD Gouge. (a) Friction versus shear displacement plot of SAFOD Gouge, talc, and quartz/montmorillonite 50/50 mixture. All experiments are performed at room temperature and a shear velocity of 0.6 μm/s using distilled water as pore fluid. The SAFOD Gouge is weaker than both talc and the quartz/montmorillonite mixture at both 10 and 100 MPa σ_n^e . (b) Friction versus shear displacement for wet and dry SAFOD Gouge. Dry SAFOD gouge has a coefficient of friction approximately 0.03 higher than wet (brine) SAFOD Gouge.

quartz/montmorillonite 50/50 mixture. In each experiment the three gouge materials reach a steady state frictional strength with minor work-hardening and work-softening.

Experiments conducted on SAFOD gouge using room dry gouge and gouge saturated in brine show that the frictional strength is affected by pore fluid. The brine saturated gouge is 17% weaker than room dry gouge (Figure 9b). The general behavior of dry and brine saturated gouge is similar, showing only slight work-hardening or work-softening after yield.

3.2.2. Velocity Dependence of SAF Gouge Friction

Steady state velocity dependence is defined as $[\Delta\mu^{ss}/\Delta(\ln V) = a - b]$, where μ^{ss} is steady state friction, V is the shear velocity, and a and b are the magnitudes of the direct and evolution effects after a velocity step, respectively [*Chester*, 1994]. The velocity dependence of SAFOD gouge friction is examined by conducting constant velocity experiments at different velocities and by step-wise change in velocity (velocity stepping) during individual experiments.

The steady state coefficient of friction determined in constant velocity experiments SG – 2 conducted at 0.6 and SG – 4 at 0.006 μm/s are 0.135 and 0.145, respectively (Figure 10), indicating that frictional strength decreases with increasing velocity, i.e., samples are velocity-weakening. The same velocity-weakening is observed when comparing the 6.0 μm/s velocity step in experiment SG – 8 to experiment SG – 2. In both comparisons, the velocity dependence a-b = -0.002.

Velocity stepping was conducted over four orders of magnitude from 6.0 to 0.006 μm/s (Figure 11), and step changes consisted of an increase or decrease in velocity

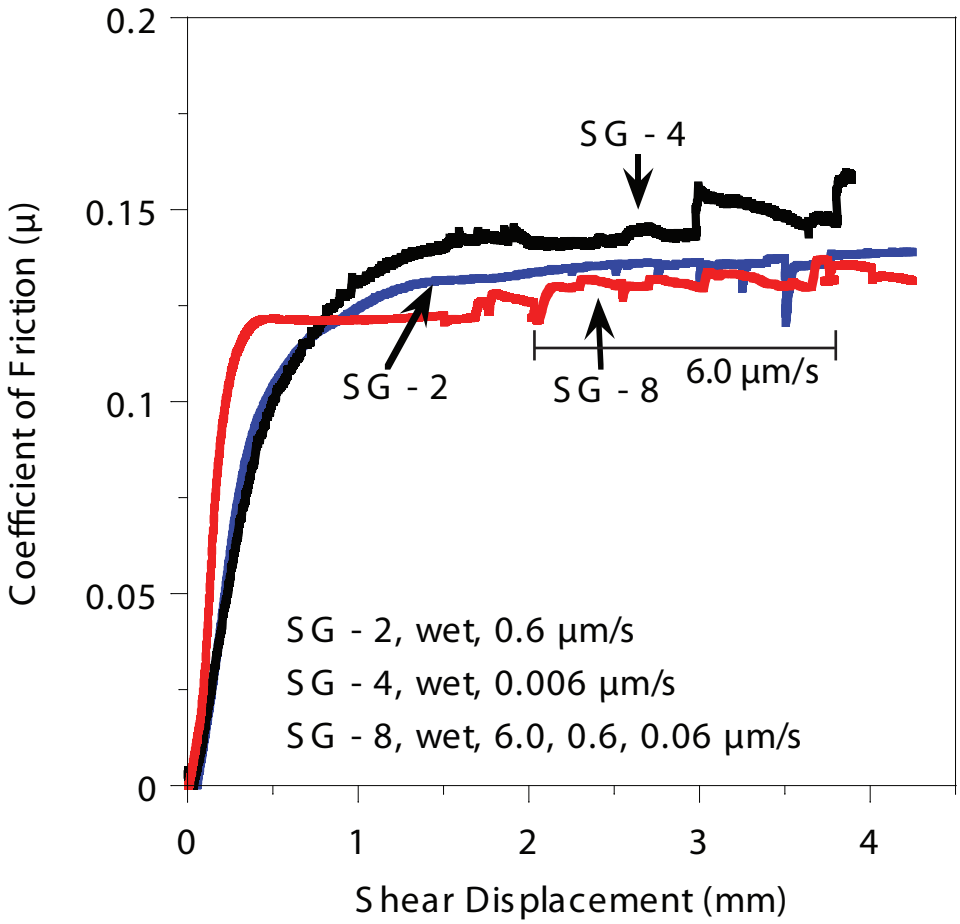

Figure 10. Coefficient of friction versus shear displacement for two constant shear velocity experiments (SG – 2 and SG – 4) and one velocity stepping experiment (SG – 8). Each experiment is conducted at in situ conditions. A decrease in frictional strength is seen as the shear velocity is increased from 0.006 μm/s (SG – 4) to 0.6 μm/s (SG – 2) to 6.0 μm/s (from 2.25 to 3.8 mm in experiment SG – 8).

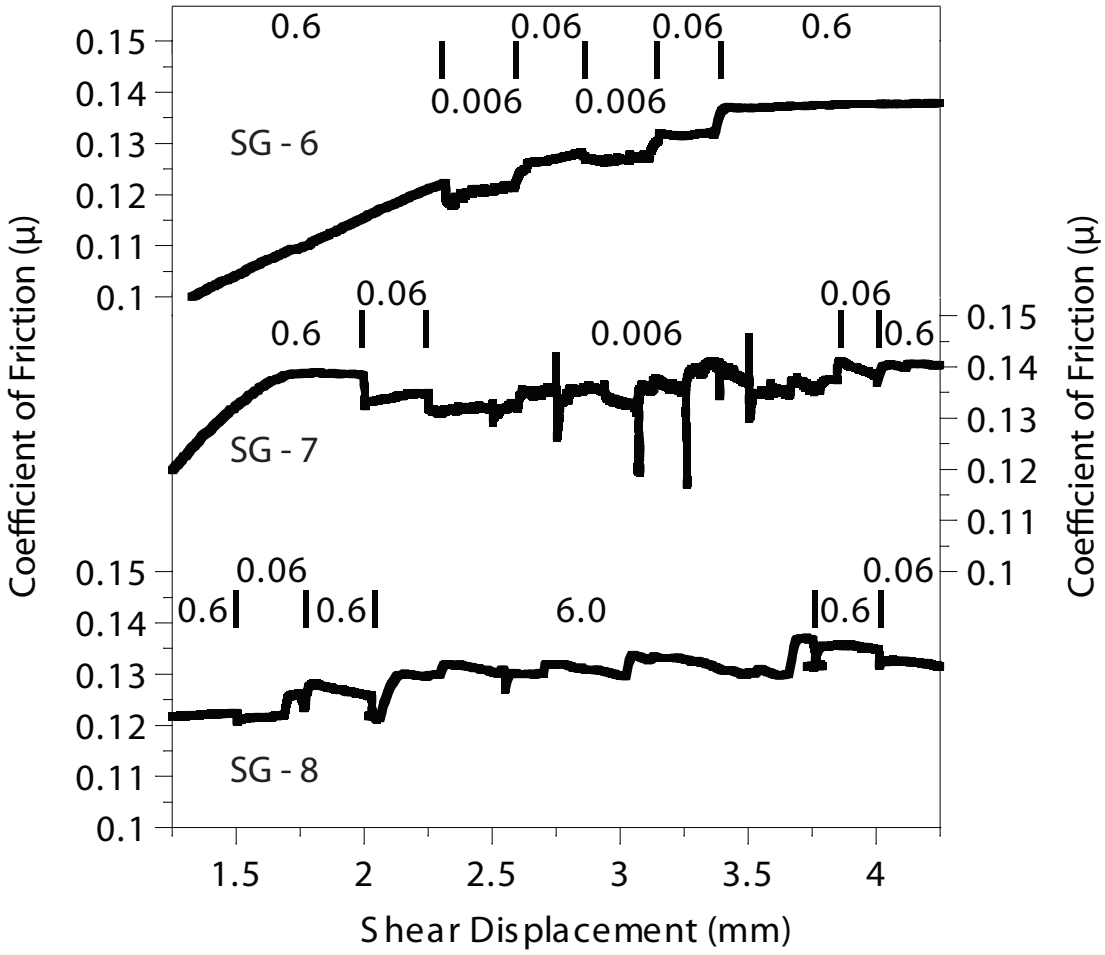

Figure 11. Coefficient of friction versus shear displacement for velocity stepping tests performed on SAFOD Gouge during experiments SG – 6, SG – 7, and SG – 8. The shear velocities (μm/s) are indicated for each experiment.

by one order of magnitude once the coefficient of friction was nearly constant. The value of a-b for each step is determined from the difference in the average coefficient of friction over the 0.025 mm of shear displacement just prior to and just after the velocity step, referred to as the "instantaneous" value, or by the difference in the average coefficient of friction spanning the 0.25 mm preceding and succeeding the velocity step, referred to as the "average" value (Figure 12). Both the a-b average and a-b instantaneous values are generally positive, i.e., velocity-strengthening, and range between -0.0017 and 0.0027 (Figure 13). The a-b values become slightly less positive as shear velocity increases, and the only negative a-b value occurred at 6.0 μm/s, the highest velocity tested.

3.2.3. Temperature Dependence of SAFOD Gouge Friction

Steady state temperature dependence is defined as

$[\Delta\mu^{ss}/\Delta(1/T) = (aQ_a - bQ_b) / R = c]$ where T is the temperature, aQ_a and bQ_b are the activation energies for the direct and evolution effects, respectively, and R is the gas constant [*Chester*, 1994]. The temperature dependence of SAFOD gouge friction was tested by stepping the temperature at 0.25 mm shear displacement intervals. The tests are conducted at the slowest velocity (0.006 μm/s) to minimize the displacement while T is equilibrating during T – steps. The initial temperature was 100°C followed by changes to 80°, 100°, 120°, and 100°C. The initial step in temperature from 100°C to 80°C shows a slight increase in the coefficient of friction, i.e. temperature-weakening. However, all subsequent step changes in temperature showed temperature-strengthening behavior (Figure 14). SG – 9, which was performed at room temperature, an effective normal

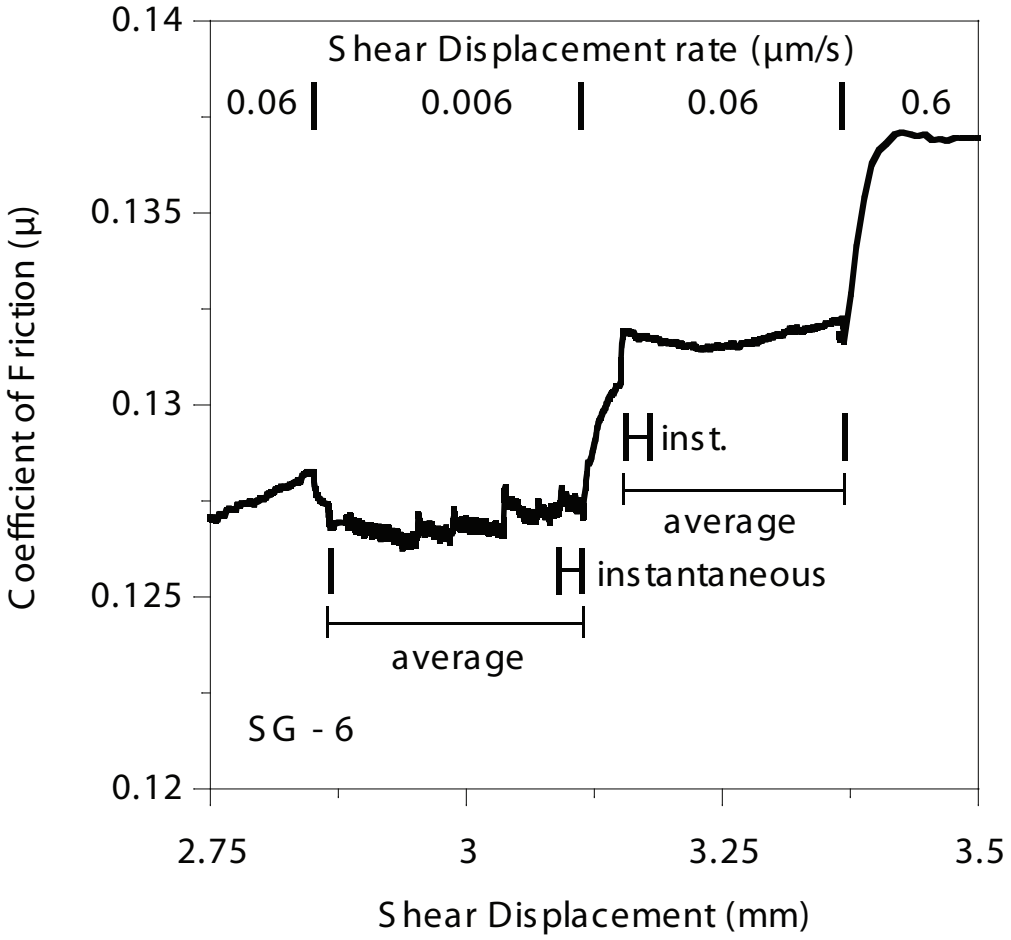

Figure 12. Displacement intervals used to determine average friction coefficient and the change in friction for velocity steps, i.e., the "a-b instantaneous" and "a-b average" values.

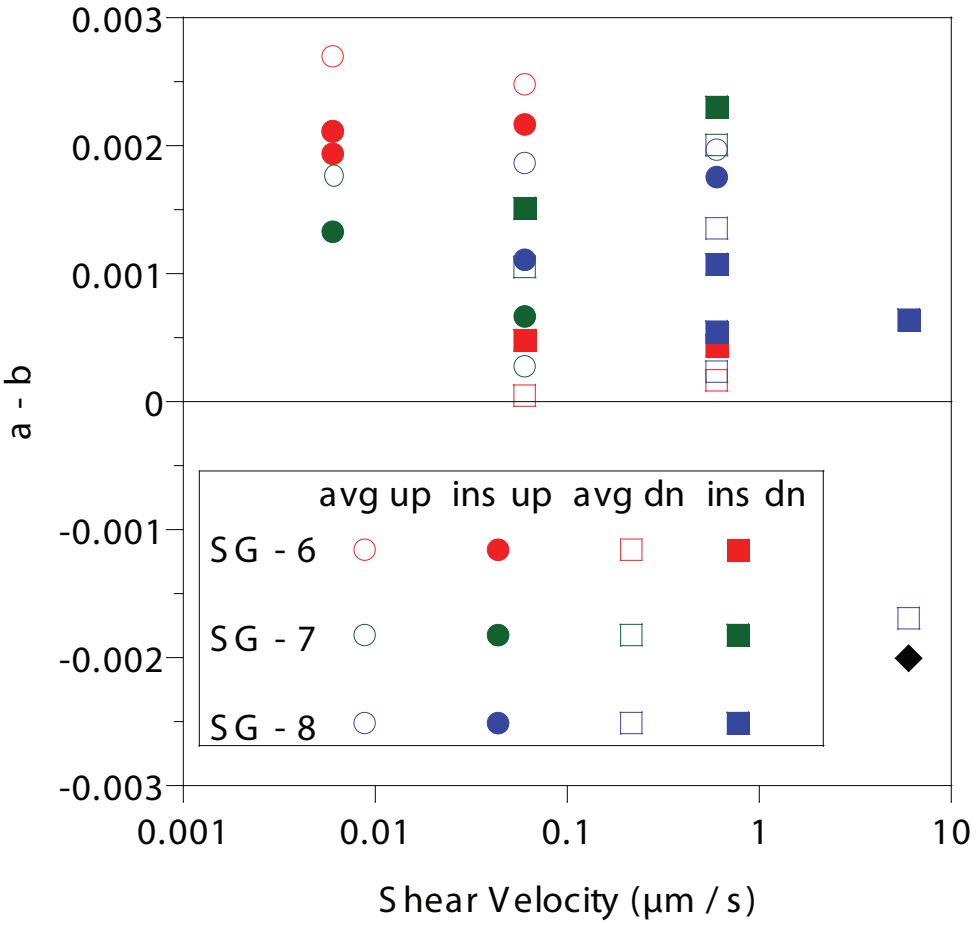

Figure 13. Velocity dependence parameters (a-b) for SAFOD Gouge versus shear velocity for experiments SG – 6, SG – 7, and SG – 8. The a-b measurements of both instantaneous and average velocity dependence (Figure 10) have a similar range of magnitudes for each velocity tested. Steps up (circles) and steps down (squares) in velocity are similar in magnitude. Generally the a-b value is positive indicating velocity-strengthening behavior. The solid diamond represents the a-b value determined during the constant velocity experiments.

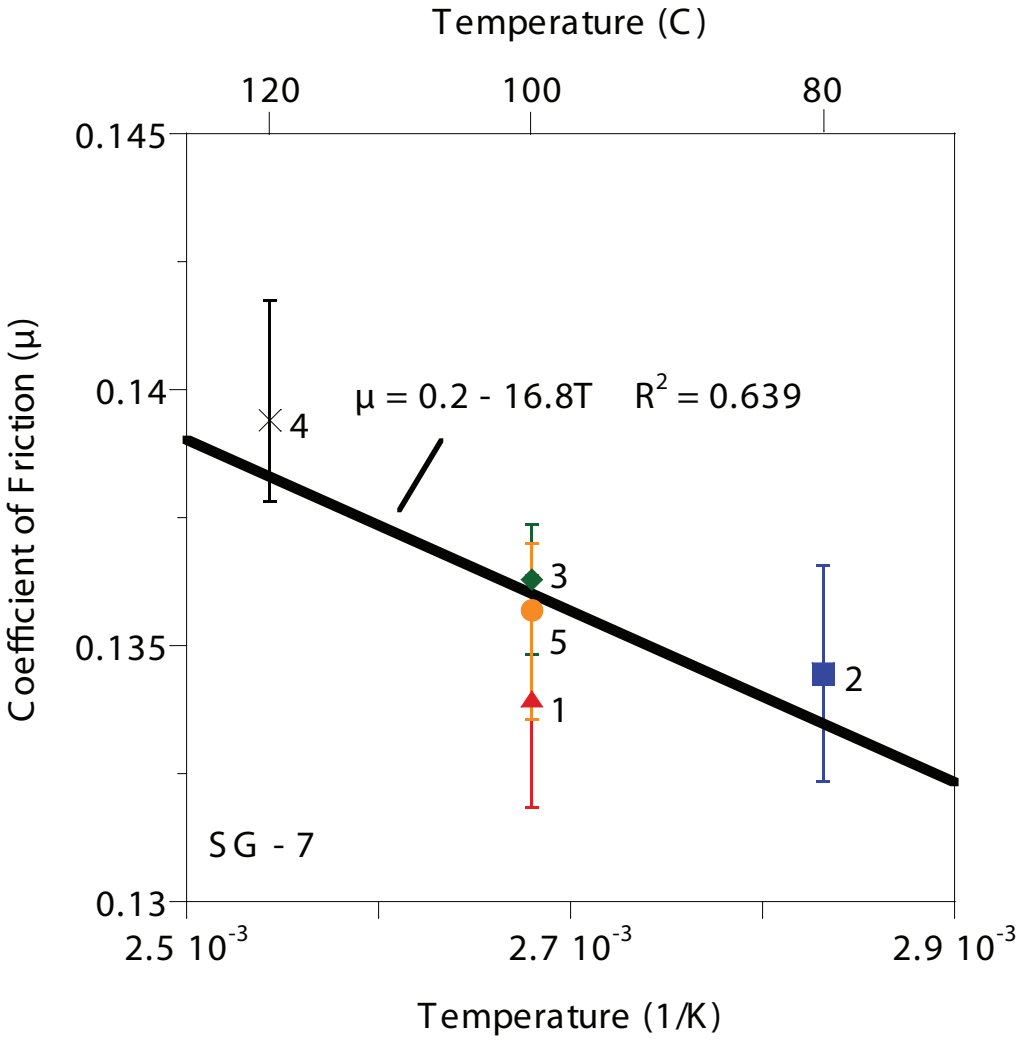

Figure 14. Coefficient of friction of SAFOD Gouge as a function of temperature for experiment SG – 7. Error bars indicate the range in coefficient of friction measured at a given temperature. Numbers indicate the temperature stepping order beginning at 1 and ending at 5. The SAFOD Gouge is characterized by temperature-strengthening behavior.

stress of 100 MPa, and with distilled water as pore fluid, is slightly weaker ($\mu = 0.12$) than the experiments performed at 100°C (average $\mu = 0.13$). This is consistent with the temperature-strengthening seen in the temperature stepping experiments.

3.2.4. Slide-Hold-Slide Tests

Due to the low stiffness of the apparatus, the transient behavior as sliding is resumed after a hold is poorly resolved. Therefore, only the relaxation behavior during the hold period of the slide-hold-slide tests is reported. Results of the slide-hold-slide tests in the Inter-laboratory Comparison Study experiments are similar for talc and the quartz/montmorillonite 50/50 mixture, as well as for the SAFOD gouge (Figure 15a). The reduction in friction during the holds is approximately three times greater at low effective normal stresses than at high normal stress. At both high and low effective normal stresses the quartz/montmorillonite 50/50 mixture shows the greatest magnitude relaxation, and talc displays the smallest magnitude relaxation.

In each experiment the reduction in the coefficient of friction increases logarithmically with hold time, and the magnitude of relaxation during a hold may be described by $a_R = \Delta\mu/\Delta(\log t)$ (Figure 15b). Of the experiments performed at an effective normal stress of 100 MPa, the room dry experiment (SG – 3) shows the largest reduction in the coefficient of friction during each hold with $a_R = 0.006$. SG – 1, which is saturated with brine, has a smaller magnitude of relaxation with $a_R = 0.002$. The largest magnitude of relaxation is observed in SG – 10 ($a_R = .009$), which was performed at an effective normal stress of 10 MPa and room temperature under saturated conditions using distilled water as pore fluid.

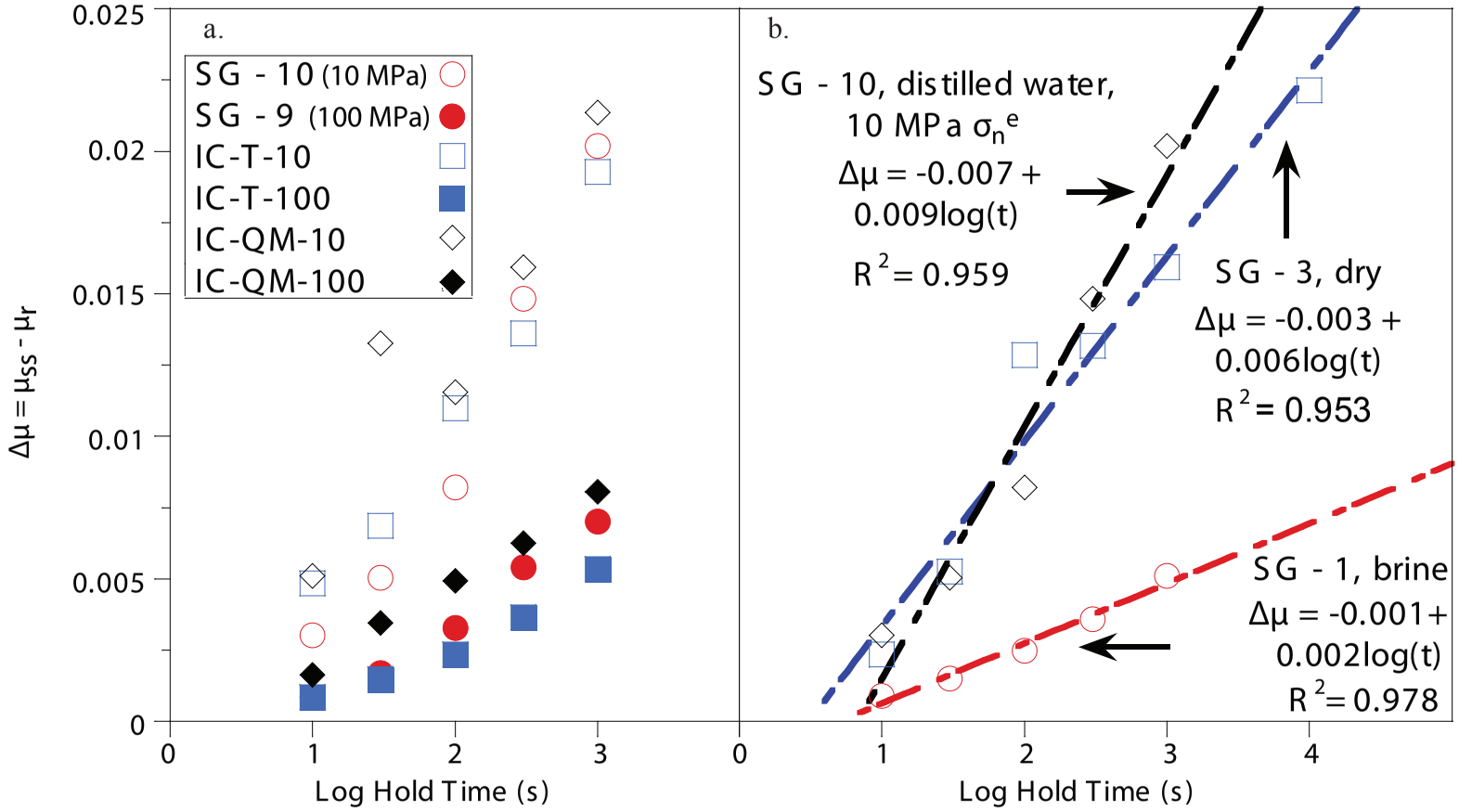

Figure 15. Plot of the change in the coefficient of friction versus hold time for slide-hold-slide test conducted on (a) talc, quartz/montmorillonite, and SAFOD Gouge experiments and (b) wet and dry SAFOD Gouge. (a) 10 MPa effective normal stress experiments are represented by open symbols and 100 MPa effective normal stress experiments are represented by closed symbols. (b) SAFOD Gouge saturated with brine has a smaller reduction in friction than room-dry SAFOD Gouge. At relatively low effective normal stresses and room temperatures the reduction in friction of SAFOD Gouge is similar to room-dry SAFOD Gouge at 100°C.

3.2.5. Pore Volume Change Within the SAFOD Gouge

The change in pore volume was monitored for several experiments on the SAFOD gouge, during equilibration at temperature and pressure prior to shearing, as well as during the shearing portion of the test. In general, all experiments show a reduction in pore volume (compaction). In each case, samples show an initially high rate of compaction that progressively diminishes to an insignificant value at about 10^4 s (Figure 16a and 16b). Particularly long duration experiments such as SG – 2, reach a constant pore volume. At times greater than 4×10^4 s, SG – 2 shows an apparent increase in pore volume that implies dilation of the gouge (Figure 16a), however, it is more likely this response reflects long-term variation in temperature of the laboratory and thermal expansion effects [Lenz, 2002]. For the shear tests incorporating holds or step changes in shear velocity, pore volume changes smoothly with time, regardless of holds or shear velocity changes, but not with shear displacement (Figure 16c). The overall response suggests small rates of pore fluid flow and long times to equilibrate relative to the duration of holds and increments of sliding between velocity steps.

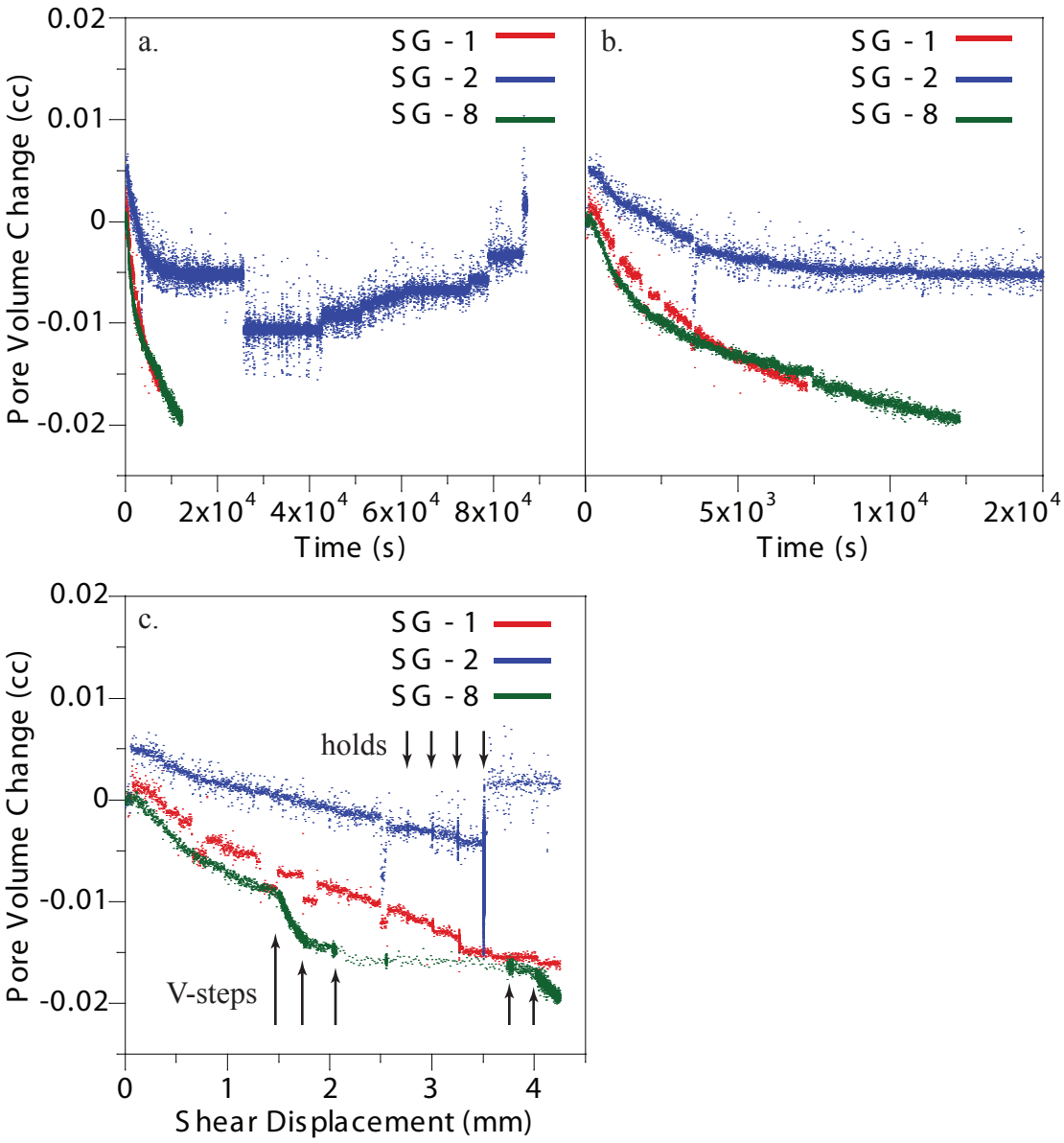

Figure 16. Pore volume change versus time (a and b) and displacement (c) for experiments SG – 1, SG – 2, and SG – 8. Negative pore volume change represents compaction, and positive pore volume change represents dilation. The gouge compacts for the duration of the shorter term experiments but appears to dilate during the 80,000 s hold in experiment SG – 8.

4. DISCUSSION

4.1. Frictional Behavior of the SAFOD Gouge

Shearing of SAFOD gouge occurs at an extremely low coefficient of friction at all the conditions tested. Similar to many other studies of simulated and natural gouge friction, the strength of the SAFOD gouge is greater at room dry conditions compared to water and brine-saturated conditions [*Rutter and Mainprice*, 1978; *Chester and Higgs*, 1992; *Chester*, 1994; *Wintsch et al.*, 1995; *Morrow et al.*, 2000; *Moore and Lockner*, 2004; *Ikari et al.*, 2007; *Moore and Lockner*, 2008; *Ikari et al.*, 2009]. Although comparison of behavior under wet and dry conditions is useful to understand the slip processes and variations in frictional strength, the room dry experiments do not have much direct relevance to the behavior of SAF gouge in situ. In contrast, it is extremely important to understand the cause of the difference in velocity dependence determined from constant velocity experiments and velocity-stepping tests in order to properly extrapolate experiment results and predict friction at in situ conditions.

The observation that the constant velocity experiments indicate velocity weakening, opposite to that observed in the velocity-stepping tests at the same conditions, may be explained by the development of non-equilibrated pore fluid pressures. Evidence of non-equilibration is seen at the beginning of each experiment as the gouge is consolidated by initial loading and onset of shear. Observations suggest that pore fluid pressure equilibration is achieved by about 4×10^4s after loading is initiated.

This time-frame for equilibration is longer than the duration of the shear experiments at velocities of 0.6 and 0.06 μm/s. Thus, at rates of 0.06 μm/s and greater, the pore pressure likely is not equilibrated. Only gouge sheared at the lowest rate of 0.006 μm/s achieves pore pressure equilibration, since the duration of this test exceeds the 40,000 s equilibration time by a factor of 10. Thus, it is only in this experiment that the measured coefficient of friction is correct in an absolute sense.

The plots of pore volume change versus time and shear displacement suggest that the expulsion of fluid and the rate of fluid expulsion with time is smoothly varying, whereas the expulsion of fluid does not correlate directly with displacement. Because one would expect that the rate of consolidation of the gouge layer should correlate with shear rate, then the changes in shear rate, and thus changes in consolidation rate, during velocity steps are apparently much faster than the characteristic times for fluid flow out of the gouge layer. Thus, a change in out-flow rate after a change in shear rate is not seen. This also suggests that pore fluid pressure is not equilibrated for shear rates of 0.06 μm/s and greater. The same is true for long holds, where holds can be distinguished in volume versus displacement plots, but not in volume versus time plots (Figure 16c).

If pore fluid is overpressured in the gouge layer, is elevated due to relatively rapid shear compaction and low permeability, then the lower frictional strength of the gouge at higher shear velocities in the constant velocity tests (apparent velocity weakening) could be due to lower effective normal stress. By assuming the true base-level coefficient of friction is given by the slowest constant-velocity experiment, and the difference in the coefficient of friction is from elevated pore fluid pressures, the

magnitude of pore fluid pressure in the faster experiments is approximately 7 MPa greater than in the slowest test.

Although the pore fluid is overpressured during the faster shear velocity experiments, the pore fluid pressure may be relatively constant during velocity stepping because the duration of velocity stepping is short relative to the pore fluid pressure equilibration time. There could be additional over or under pressurization caused by the step changes in velocity. If so, different magnitudes of a-b values for steps up relative to steps down would be expected. Observations of similar a-b values for steps up and steps down in velocity suggest additional over or under pressurization is relatively small. Therefore, the observed a-b values for SAFOD gouge from the stepping experiments are considered valid.

For temperature stepping tests in experiment SG – 7, the pore fluid pressure is allowed to equilibrate at a shear velocity of 0.006 μm/s prior to the steps. Once the characteristic time for pore fluid pressures to equilibrate has elapsed, the measurements of friction for the temperature stepping test should be accurate. The initial temperature step in SG – 7 is recorded before the required equilibration time elapsed, possibly leading to the slightly lower value, whereas all the other measurements are internally consistent.

4.2. Comparison of SAFOD Gouge Behavior to Other Weak Materials

The low frictional strength of the SAFOD gouge is similar to the strength of several weak minerals including sheet silicates such as smectites (montmorillonite), the serpentine mineral chrysotile, and talc. These minerals have been found to have some of

the lowest frictional strengths observed (μ = 0.08 to 0.5) [*Logan and Rauenzahn*, 1987; *Reinen et al.*, 1991; 1994; *Moore et al.*, 1997; *Saffer and Marone*, 2003; *Moore and Lockner*, 2004; *Moore and Rymer*, 2007; *Moore and Lockner*, 2008; *Carpenter et al.*, 2009; *Ikari et al.*, 2009; *Tembe et al.*, 2010]. These minerals occur within the SAFOD gouge [*Solum et al.*, 2006; *Moore and Rymer*, 2007]. *Logan and Rauenzahn* [1987] found that the coefficient of friction for montmorillonite is between 0.08 and 0.14 at room temperature, confining pressures of 25 to 75 MPa, and slip rates of 0.001 to 100 μm/s. *Reinen et al.* [1994] found that chrysotile serpentinite has a coefficient of friction of 0.15 to 0.35 during experiments at room temperature, confining pressure of 25 to 75 MPa, and slip rates of 0.001 to 10.0 μm/s. *Moore et al.* [1997] determined that chrysoltile serpentine has a coefficient of friction of 0.1 to 0.2 up to 100°C but strengthens at higher temperatures as adsorbed water is removed. *Saffer and Marone* [2003] found that the coefficient of friction for smectites at room temperature is less than 0.2 at normal stresses between 40 and 150 MPa and sliding velocities from 1.0 to 200 μm/s. *Moore and Lockner* [2008] discovered that water saturated talc is weak ($\mu < 0.2$) from room temperature to 400°C, and normal stresses from 25 to 300 MPa. *Carpenter et al.* [2009] found that water saturated serpentine from near the SAF has a coefficient of friction of 0.18 to 0.24 at room temperature, normal stresses of 4 to 100 MPa, and slip rates from 1 to 300 μm/s.

The SAFOD gouge is much weaker than previously tested materials from the SAF at SAFOD performed at similar shear velocities, which includes drill cuttings taken over the length of the borehole [*Tembe et al.*, 2006; *Morrow et al.*, 2007; *Carpenter et*

al., 2009], and fault rock samples from shear zones intersected by the borehole [*Tembe et al.*, 2009]. *Tembe et al.* [2006] deformed cuttings from the depth interval of 1.85 to 3.1 km. *Morrow et al.* [2007] used geophysical logs to determine the location of shear zones and selected only cuttings that displayed striations, taken as evidence of shearing. The cuttings with striations are weaker (μ = 0.25 to 0.48) than cuttings without striations (μ = 0.4 to 0.8) [*Tembe et al.*, 2006]. Cuttings taken from a fault intersected by the borehole at 2521 m measured depth are weaker (μ = 0.25 – 0.35) than cuttings taken from near the CDZ (μ = 0.35 – 0.5) [*Morrow et al*., 2007]. XRD analysis showed that the cuttings from near the CDZ have a higher percentage of strong minerals such as quartz and albite, while the cuttings from the 2521 m fault have a higher percentage of chlorite, illite, and mixed illite/montmorillonite.

The SAFOD Cuttings tested in the SAFOD Inter-laboratory Comparison study were collected from a shale unit ranging from 3160 to 3179 m measured depth, and not necessarily from shear zones. The frictional strength of the SAFOD Cuttings from this study (μ = 0.6 – 0.7) is similar to the frictional strength found in other studies for cuttings with no evidence of shear [*Tembe et al.*, 2006; *Morrow et al.*, 2007; *Carpenter et al.*, 2009].

Tembe et al. [2009] conducted triaxial friction experiments on a black gouge taken from a minor, inactive fault in the arkosic sandstone of the western damage zone at 3067 m measured depth. These tests were performed at temperatures ranging from 96° to 431°C, effective normal stresses of 38 to 300 MPa, axial displacement rate of 0.05 to 0.5 μm/s, and a pore fluid pressure of 100 MPa using deionized water. Friction of the black

gouge ranged from 0.4 to 0.73, and the lowest coefficient of friction was found at 100°C and 75 MPa effective normal stress, conditions similar to those used in this study. However, the black gouge from the minor, inactive strand of the SAF is not as weak as the SAFOD gouge from the CDZ. *Tembe et al.* [2009] reported the mineralogy of the black gouge as being 48–51 % illite, 14–18% mixed illite-smectite, 19–22% feldspar, 11–17% quartz, 1% chlorite, and trace amounts of calcite. High-speed friction experiments (shear velocity = 1.3 m/s) performed on water-dampened, disaggregated material from the 3067 m fault have found extremely low coefficient of friction values ($\mu = 0.15$) [*Kitajima et al*., manuscript in preperation, 2010]. However, at high shear velocities, weakening mechanisms would not be similar to the deformation mechanisms that occur at the low shear velocities used by *Tembe et al*., [2009].

The SAFOD gouge used herein is clay-rich with visible clasts of serpentinite as well as small amounts of talc. A stated above, previous studies on clays such as montmorillonite, talc, and the serpentine mineral chrysotile have found that these minerals have low coefficients of fiction ($\mu = 0.2$ to 0.5) [*Reinen et al.*, 1991; 1994; *Morrow et al.*, 2000; *Saffer and Marone*, 2003; *Moore and Lockner*, 2004; *Ikari et al.*, 2007; *Moore and Lockner*, 2008; *Ikari et al.*, 2009; *Tembe et al.*, 2010]. The occurrence of these minerals within the SAFOD gouge likely contributes to the low coefficient of friction observed in this study.

Generally, velocity-strengthening behavior is observed in the SAFOD gouge. The values of a-b in this study (-0.0017 to 0.0027) are similar to values from several other studies with clay rich gouge [*Saffer and Marone*, 2003; *Tembe et al.*, 2006;

Morrow et al., 2007; *Moore and Lockner*, 2008; *Carpenter et al.*, 2009; *Ikari et al.*, 2009; *Tembe et al.*, 2010]. In particular, the a-b values determined in this study are similar to values determined for both smectite and illite gouge [*Saffer and Marone*, 2003]. The cuttings from the SAFOD borehole also show a similar velocity dependence [*Morrow et al.*, 2007; *Carpenter et al.*, 2009]. *Tembe et al.* [2009] found that the black gouge used in velocity stepping tests transitioned from velocity-strengthening at low temperatures ($T < 266°C$) to velocity-weakening at intermediate temperatures ($266°C \leq T \leq 283°C$) to velocity-strengthening at high temperatures ($> 283°C$). For the SAFOD gouge, as the velocity increases the a-b value is reduced. Based on the trend of the velocity dependence data, the possibility remains that at higher velocities the SAFOD gouge could transition to velocity-weakening behavior. The velocity-strengthening behavior of the SAFOD gouge, at the low velocities tested in this study, is consistent with the aseismic, creeping behavior of the central section of the SAF. Extrapolating the velocity-strengthening behavior to the slip-rate of the creeping section of the SAF leads to greater velocity-strengthening.

While previous friction studies have found temperature-weakening in quartz gouge [*Chester*, 1994], this study demonstrates that the clay-rich SAFOD gouge is temperature-strengthening. Temperature-weakening in quartz represents a transition in deformation mechanisms from pressure dependent cataclasis to time-and temperature-dependent solution transfer and crystal plasticity. Temperature-strengthening of clay-rich gouge, such as the SAFOD gouge, is possibly the result of the loss of adsorbed water from the surfaces of sheet structured silicates, such as clays, serpentines, and talc [*Moore*

et al., 1997; *Morrow et al.*, 2000; *Moore and Lockner*, 2004; 2008]. Temperature-strengthening behavior of the SAFOD gouge is consistent with results from another study on gouge taken from the 3067 m measured depth fault, a subsidiary fault, intersected by the borehole at SAFOD [*Tembe et al.,* 2009]. Illite and the serpentine mineral chrysotile have been found to become stronger as temperature is increased [*Moore et al*., 1989; 1997]. A similar increase in frictional strength is seen for dried gouge [*Morrow et al.*, 2000; *Moore and Lockner*, 2004]. As with heated clay-rich gouge, the drying of gouge causes the interlayer water to be removed. Our experiments confirm that room dry samples, such as SG – 3, are stronger than experiments performed in the presence of distilled water or brine.

As noted in the previous section, evidence suggests that over pressurization of the pore fluid at shear velocities of 0.06 μm/s and faster result in a reduction of the frictional strength. This is particularly true if the time for pore fluid pressure equilibration prior to shearing is not long enough. Previous studies using clay-rich gouge, as well as studies on SAFOD materials, generally are conducted at rates greater than 0.06 μm/s. Therefore, these studies may not allow adequate time for pore fluid equilibration that is determined herein [*Moore et al*., 1989; *Morrow et al*., 1992; 2000; *Moore and Lockner*, 2004; *Tembe et al*., 2010]. Without verifying the permeability, it is possible that these studies develop excess pore fluid pressures within the gouge layer. Excess pore fluid pressure would lead to an under estimation of the coefficient of friction, similar to this study.

4.3. Frictional Strength of San Andreas Fault at SAFOD

The results of this study show that the SAFOD gouge taken from the actively deforming CDZ has the lowest frictional strength, by far, of all SAFOD materials tested [*Tembe et al*., 2006; *Morrow et al*., 2007; *Carpenter et al*., 2009; *Tembe et al*., 2009]. The low frictional strength of the CDZ gouge layer is likely the reason that deformation is concentrated in this region of highly foliated gouge. The foliated fabric of the SAFOD gouge has been documented by *Sills et al.* [2009]. Using X-ray Computed Tomography they found a shape preferred orientation of porphyroclasts that persist to the sub-millimeter size. A clay foliation can be seen with the unaided eye, as well, in the Phase III Core Atlas Ver. 4 (http://www.earthscope.org/es_doc/data/safod/Core%20Photo%20Atlas%20v4.pdf). The gouge is noted in the Core Atlas as having a "wavy foliation" and a "micro-scaly fabric". To try to preserve the fabric and pophyroclasts, the SAFOD gouge was lightly disaggregated and relatively large diameter particles were retained (up to 844 μm). Although the meso-scale fabric was not retained during disaggregation, the large particle size allowed the microscale fabric to be retained. The preservation of the microscale fabric is important to most accurately determine the frictional strength of the SAFOD gouge. Recent experimental studies show that fabric plays a role in lowering the frictional strength of fault gouge [*Collettini et al.*, 2009; *Niemeijer et al.*, 2010]. When the fault gouge fabric is preserved, slip is localized within the preexisting foliation containing weak minerals [*Collettini et al.*, 2009], and can lower the coefficient of friction by as much as 0.3 [*Collettini et al.*, 2009; *Niemeijer et al.*, 2010]. Smectite coatings along interconnected fractures have been observed within the CDZ allowing for

slip to be accommodated entirely within these weak micro-shear zones [*Schleicher et al*., 2010]. It is possible that the low frictional strength observed in this study partially reflects fabric weakening. To determine the effect of the fabric on frictional strength, future experiments should be conducted on SAFOD gouge disaggregated to a particle size of less than 190 μm. Also, a microstructual study should be done to determine if slip is accommodated within shear zones lined with low strength minerals.

The shear velocities employed herein, while slower than most friction studies, are faster than the shear velocities seen along the SAF at SAFOD. The shear velocities used in this study of 0.006 to 6.0 μm/s correlate to a shear strain rate of 3.0×10^{-6} to 3.0×10^{-3} s^{-1} (gouge layer thickness is 2 mm). Using the measured displacement rate for the region near SAFOD of 30 mm/yr [*Titus et al.*, 2006] and the 4 m combined thickness of the SDZ (1.6 m) and CDZ (2.6 m) gouge zones, the shear strain rate for the SAF is 2.4×10^{-10}. Taking the base level coefficient of friction value of 0.143 at 0.006 μm/s (SG – 4) and using the velocity dependence determined for the SAFOD gouge, the coefficient of friction calculated for the strain rate of the SAF is 0.129. If the strain rate fluctuates as the result of laterally varying gouge thickness, or from the possible presence of additional creeping traces further east, the coefficient of friction would decrease further.

Measurements of stress orientations near the SAF have shown that the maximum horizontal compressive stress, σ_{Hmax}, is nearly normal to the SAF [*Mount and Suppe*, 1987; *Zoback et al*., 1987; *Provost and Houston*, 2001; *Hickman and Zoback*, 2004]. Data from this study supports the idea that slip along the SAF can occur with σ_{Hmax} at these orientations. Given the magnitude of the maximum and minimum horizontal

principal compressive stress of 113 and 49 MPa, respectively, determined by *Hickman and Zoback* [2004] at 1671 m depth in the SAFOD pilot hole, and using the coefficient of friction determined in this study calculated for the strain rate of the creeping section of the SAF (0.129), the orientation of the maximum horizontal compressive stress that would permit slip can be as high as 84° to the plane of the SAF (Figure 17). Assuming a maximum horizontal principal compressive stress orientation of 70° to the SAF, *Tembe et al*. [2009] determined that for a coefficient of friction greater than 0.2, excess pore pressure would be necessary to allow for slip on the SAF. The coefficient of friction of the SAFOD gouge reported here allows for slip to take place regardless of excess pore pressure.

The coefficient of friction determined for the SAFOD gouge is at the upper limit of the heat flow constraint. *Brune* [1969] and *Lachenbruch and Sass* [1980] determined that the strength of the SAF must be approximately 10 MPa based on the lack of a frictionally generated heat flow. The possibility exists that at slower shear velocities or at higher temperatures other weakening mechanisms such as dissolution-aided slip or dislocation creep may allow for further weakening of the SAFOD gouge.

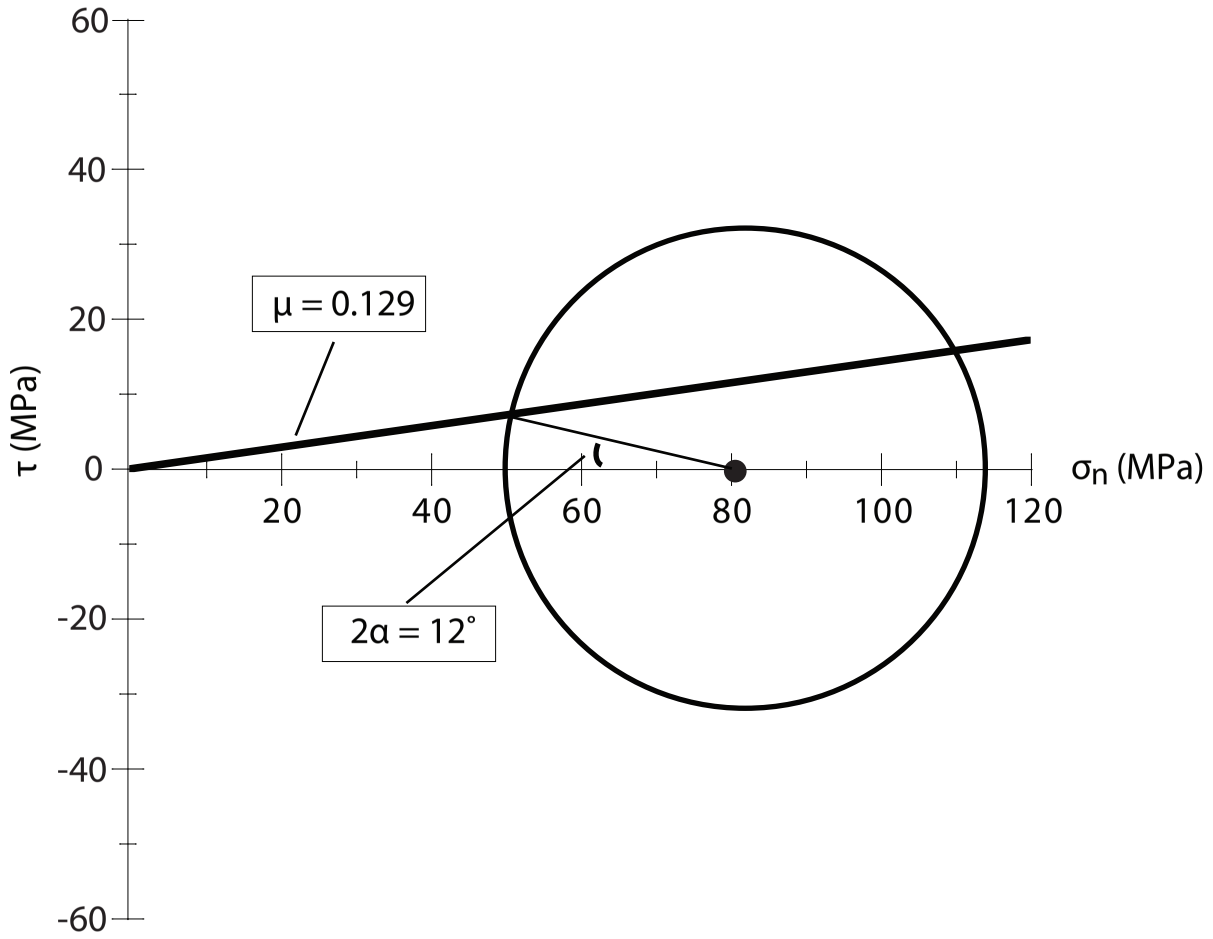

Figure 17. Mohr circle diagram depicting the orientation at which the maximum horizontal principal compressive stress allows for slip to occur on the SAF. The coefficient of friction is 0.129 and maximum and minimum horizontal principal compressive stresses are 113 and 49 MPa, respectively. Slip can occur if the maximum horizontal principal compressive stress is oriented at 90º - α to the SAF plane.

5. CONCLUSIONS

1) The SAFOD gouge is extremely weak ($\mu = 0.145$) when tested at in situ temperature (100°C), pressure (100 MPa σ_n^e), and pore fluid chemistry (Ca-Na-K brine) present at SAFOD. The low coefficient of friction of the SAFOD gouge satisfies the apparent low frictional strength of the SAF based on heat flow and stress orientation measurements

2) Room dry SAFOD gouge, is slightly stronger than water saturated SAFOD gouge. At the conditions tested, the SAFOD gouge samples saturated with distilled water have similar strengths as those saturated with brine.

3) The SAFOD gouge shows stable, rate-strengthening behavior at the conditions and rates tested. Rate-strengthening behavior is consistent with the aseismic creep on the SAF at SAFOD.

4) Temperature-strengthening behavior is observed for the SAFOD gouge, and may reflect loss of interlayer water from clay minerals, consistent with the frictional behavior of clay-bearing gouge determined in previous experimental studies.

5) The combination of weak mineral components (montmorillonite and serpentinite) and the micro-foliated fabric that allow for slip to be localized within micro-shear zones can explain the extremely low frictional strength of the SAFOD gouge.

6) Room temperature experiments conducted on SAFOD gouge, at effective normal stresses of 10 and 100 MPa, and using distilled water as pore fluid, also are weak. The

frictional strength of the SAFOD gouge is similar to the talc and quartz/montmorillonite gouge tested as part of the SAFOD Inter-laboratory Comparison Study.

REFERENCES

Allen, C. R. (1968), The tectonic environments of seismically active and inactive areas along the San Andreas fault system, in *Proc. of the Conference on Geologic Problems of the San Andreas Fault System,* edited by W. R. Dickinson and A. Grantz, *Stanford Univ. Publ. Geol. Sci.*, *11*, 70–82.

Beeler, N. M., T. E. Tullis, and J. D. Weeks (1994), The roles of time and displacement in the evolution effect in rock friction, *Geophys. Res. Lett.*, *21*, 1987-1990.

Beeler, N. M., T. E. Tullis, M. L. Blanpied, and J. D. Weeks (1996), Frictional behavior of large displacement experimental faults, *J. Geophys. Res.*, *101*, 8697-8715.

Bos, B., C. J. Peach, and C. J. Spiers (2000), Frictional-viscous flow of simulated fault gouge caused by the combined effects of phyllosilicates and pressure solution, *Tectonophysics, 327*, 173-194.

Brown, R. D., Jr., and R. E. Wallace (1968), Current and historic fault movement along the San Andreas fault between Paicines and Camp Dix, California, in *Proc. of the Conference on Geologic Problems of the San Andreas Fault System,* edited by W. R. Dickinson and A. Grantz, *Stanford Univ. Publ. Geol. Sci., 11*, 22–39.

Brune, J. N., T. L. Henyey, and R. F. Roy (1969), Heat flow, stress, and rate of slip along San Adreas Fault, California, *J. Geophys. Res., 74*, 3821-3827.

Byerlee, J. D., and W. F. Brace (1972), Fault stability and pore pressure, *Bull. Seismol. Soc. Amer., 62*, 657-660.

Byerlee, J. (1978), Friction of rocks, *Pure Appl. Geophys., 116*, 615-626.

Byerlee, J. D. (1990), Friction, overpressure, and fault normal compression, *Geophys. Res. Lett.*, 17, 2109– 2112, doi:10.1029/GL017i012p02109.

Carpenter, B. M., C. Marone, and D. M. Saffer (2009), Frictional behavior of materials in the 3D SAFOD volume, *Geophys. Res. Lett*., 36, L05302, doi:10.1029/2008GL036660.

Che´ry, J., M. D. Zoback, and S. Hickman (2004), A mechanical model of the San Andreas fault and SAFOD Pilot Hole stress measurements, *Geophys. Res. Lett*., 31, L15S13, doi:10.1029/2004GL019521.

Chester, F. M., and J. M. Logan (1986), Implications for mchanical-properties of brittle faults from observations of the Punchbowl Fualt zone, California, *Pure Appl. Geophys., 124*, 79-106.

Chester, F. M. (1988), The brittle-ductile transition in a deformation-mechanism map for halite, *Tectonophysics, 154*, 125-136.

Chester, F. M. (1989), Dynamic recrystallizationin semi-brittlef aults, *J. Struct. Geol*., 11, 847-858.

Chester, F. M., J. P. Evans, and R. L. Biegel (1993), Internal structure and weakening mechanisms of the San Andreas Fault, *J. Geophys. Res., 98*, 771-786.

Chester, F. M. (1994), Effects of temperature on friction: Constitutive-equations and experiments with quartz gouge, *J. Geophys. Res., 99*, 7247-7261.

Chester, J.S., F.M. Chester, D.L. Kirschner, R. Almeida, J.P. Evans, R.N. Guillemette, S. Hickman, M. Zoback, W. Ellsworth (2007), Deformation of sedimentary rock across the San Andreas fault zone: Mesoscale and microscale structures displayed in core from SAFOD, *Eos Trans. AGU*, *88*(52), T42C-05.

Collettini, C., A. Niemeijer, C. Viti, and C. Marone (2009), Fault zone fabric and fault weakness, *Nature, 462*, 907-910, doi: 10.1038/nature08585.

Escartin, J., M. Andreani, G. Hirth, and B. Evans (2008), Relationships between the microstructural evolution and the rheology of talc at elevated pressures and temperatures, *Earth Planet. Sci. Lett.*, *268*, 463-475, doi: 10.1016/j.epsl.2008.02.004.

Evans, J. P., and F. M. Chester (1995), Fluid-rock interaction in faults of the San Andreas system: Inferences from San Gabriel fault rock geochemistry and microstructures, *J. Geophys. Res.*, *100*, 13007-13020.

Heard, H. C. (1963), Effect of large changes in strain rate in the experimental deformation of Yule Marble, *J. Geol*., 71, 162–195.

Hickman, S., M. Zoback, and W. Ellsworth (2004), Introduction to special section: Preparing for the San Andreas Fault Observatory at Depth, *Geophys. Res. Lett.*, 31, L12S01, doi: 10.1029/2004GL020688.

Hickman, S., and M. Zoback (2004), Stress orientations and magnitudes in the SAFOD pilot hole, *Geophys. Res. Lett.*, 31, L15S12, doi:10.1029/2004GL020043.

Hickman, S. H., and B. Evans (1995), Kinetics of pressure solution at halite-silica interfaces and intergranular clay films, *J. Geophys. Res., 100*, 13113-13132.

Ikari, M. J., D. M. Saffer, and C. Marone (2009), Frictional and hydrologic properties of clay-rich fault gouge, *J. Geophys. Res*., 114, B05409, doi: 10.1029/2008JB006089.

Lachenbruch, A. H. (1980), Frictional heating, fluid pressure, and the resistance to fault motion, *J. Geophys. Res.*, *85*, 6097-6112.

Lachenbruch, A. H., and J. H. Sass (1980), Heat-flow and energetics of the San-Andreas fault zone, *J. Geophys. Res., 85*, 6185-6222.

Lenz, S. C. (2002), Subcritical crack growth in creep compaction experiments, M.S. thesis, 62 pp., Texas A&M Univ., College Station, Tex.

Logan, J. M., and K. A. Rauenzahn (1987), Frictional dependence of gouge mixtures of quartz and montmorillonite on velocity, composition, and fabric, *Tectonophysics*, *144*(1-3), 87-108.

Marone, C. (1998a), Laboratory-derived friction laws and their applicationto seismic faulting, *Annu. Rev. Earth Planet. Sci*., 26, 643– 696.

Marone, C. (1998b), The effect of loading rate on static friction and the rateof fault healing during the earthquake cycle, *Nature*, 391, 69– 72.

Marone, C., and C. H. Scholz (1988), The depth of seismic faulting and the upper transition from stable to unstable slip regimes, *Geophys. Res. Lett*., 15, 621–624.

Moore, D. E., R. Summers, and J. D. Byerlee (1989), Sliding behavior and deformation textures of heated illite gouge, *J. Struct. Geol*., 11, 329– 342.

Moore, D. E., D. A. Lockner, S. Ma, R. Summers, and J. D. Byerlee (1997), Strengths of serpentinite gouges at elevated temperatures, *J. Geophys. Res*., 102, 14,787–14,801.

Moore, D. E., and D. A. Lockner (2004), Crystallographic controls on the frictional behavior of dry and water-saturated sheet structure minerals, *J. Geophys. Res*., 109, B03401, doi:10.1029/2003JB002582.

Moore, D. E., and M. J. Rymer (2007), Talc-bearing serpentinite and the creeping section of the San Andreas fault, *Nature, 448,* 795-797, doi: 10.1038/nature06064.

Moore, D. E., and D. A. Lockner (2008), Talc friction in the temperature range 25°-400°C: Relevance for fault-zone weakening, *Tectonophysics, 449*, 120-132, doi: 10.1016/j.tecto.2007.11.039.

Morrow, C., J. Solum, S. Tembe, D. Lockner, and T.-F. Wong (2007), Using drill cutting separates to estimate the strength of narrow shear zones at SAFOD, *Geophys. Res. Lett.*, 34, L11301, doi:10.1029/2007GL029665.

Morrow, C. A., D. E. Moore, and D. A. Lockner (2000), The effect of mineral bond strength and adsorbed water on fault gouge frictional strength, *Geophys. Res. Lett., 27,* 815-818.

Mount, V. S., and J. Suppe (1987), State of stress near the San Andreas Fault: Implications for wrench tectonics, *Geology, 15*, 1143-1146.

Niemeijer, A., C. Marone, and D. Elsworth (2010), Fabric induced weakness of tectonic faults, *Geophys. Res. Lett*., 37, L03304, doi:10.1029/2009GL041689.

Noda, H., E. M. Dunham, and J. R. Rice (2009), Earthquake ruptures with thermal weakening and the operation of major faults at low overall stress levels, *J. Geophys. Res*., 114, B07302, doi:10.1029/2008JB006143.

Numelin, T., C. Marone, and E. Kirby (2007), Frictional properties of natural fault gouge from a lowangle normal fault, Panamint Valley, California, *Tectonics*, 26, TC2004, doi:10.1029/2005TC001916.

Provost, A. S., and H. Houston (2001), Orientation of the stress field surrounding the creeping section of the San Andreas Fault: Evidence for a narrow mechanically weak fault zone, *J. Geophys. Res., 106*, 11373-11386.

Reinen, L. A., J. D. Weeks, and T. E. Tullis (1991), The frictional behavior of serpentinite: Implications for aseismic creep on shallow crustal faults, *Geophys. Res. Lett., 18*, 1921-1924.

Reinen, L. A., J. D. Weeks, and T. E. Tullis (1994), Ther frictional behavior of lizardite and antigorite serpentinites: Experiments, constitutive models, and implications for natural faults, *Pure Appl. Geophys., 143*, 317-358.

Rice, J. R. (1992), Fault stress states, pore pressure distributions, and theweakness of the San Andreas Fault, in *Fault Mechanics and Transport Properties of Rocks*, edited by B. Evans and T.-f. Wong, pp. 475– 504, Academic, San Diego, Calif.

Rice, J. R. (2006), Heating and weakening of faults during earthquake slip, *J. Geophys. Res.*, 111, B05311, doi:10.1029/2005JB004006.

Rutter, E. H., and D. H. Mainprice (1978), Effect of water on stress relaxation of faulted and un-faulted sandstone, *Pure Appl. Geophys., 116*, 634-654.

Rutter, E. H. (1983), Pressure solution in nature, theory, and experiment, *J. Geol. Soc.*, *140*, 725-740.

Rutter, E. H., R. H. Maddock, S. H. Hall, and S. H. White (1986), Comparative microstructures of natural and experimentally produced clay-bearing fault gouges, *Pure Appl. Geophys.*, *124*, 3-30.

Saffer, D. M., and C. Marone (2003), Comparison of smectite- and illite-rich gouge frictional properties: application to the updip limit of the seismogenic zone along subduction megathrusts, *Earth Planet. Sci. Lett.*, *215*, 219-235, doi: 10.1016/s0012-821x(03)00424-2.

Schleicher, A. M., B. A. van der Pluijm, J. G. Solum,and L. N. Warr (2006), Origin and significance of clay-coated fractures in mudrock fragments of the SAFOD borehole (Parkfield, California), *Geophys. Res. Lett*., 33, L16313, doi:10.1029/2006GL026505.

Schleicher, A. M., B. A. van der Pluijm, and L. N. Warr (2010), Nanocoatings of clay and creep of the San Andreas fault at Parkfield, California, *Geology*, *38*, 667-670, doi: 10.1130/G31091.1.

Scholz, C. H. (1998), Earthquakes and friction laws, *Nature*, 391, 37– 42.

Shea,W. T., and A. K. Kronenberg, (1992) Rheology and deformation mechanisms of an isotropic mica schist, *J. Geophys. Res*., 97, 15,201– 15,237.

Sibson, R. H. (1977), Kinetic shear resistance, fluid pressures, and radiation efficiency during seismic faulting, *Pure Appl. Geophys.*, *115*, 387-400.

Sibson, R. H. (1992), Implications of fault-valve behavior for rupture nucleation and recurrence, *Tectonophysics, 211*, 283-293.

Sills, D.W., J.S. Chester, F.M. Chester (2009), Shape preferred orientation of porphyroclasts in the Active Gouge Zones of the San Andreas Fault at SAFOD, *Eos Trans. AGU, 90* (52), Fall Meet. Suppl., Abstract T43A-2057.

Smith, S. A. F., and D. R. Faulkner (2010), Laboratory measurements of the frictional properties of the Zuccale low-angle normal fault, Elba Island, Italy, *J. Geophys. Res*., 115, B02407, doi:10.1029/2008JB006274.

Solum, J. G., S. H. Hickman, D. A. Lockner, D. E. Moore, B. A. van der Pluijm, A. M. Schleicher, and J. P. Evans (2006), Mineralogical characterization of protolith and fault rocks from the SAFOD Main Hole, *Geophys. Res. Lett*., 33, L21314, doi:10.1029/2006GL027285.

Tembe, S., D. A. Lockner, J. G. Solum, C. A. Morrow, T. Wong, and D. E. Moore (2006), Frictional strength of cuttings and core from SAFOD drillhole phases 1 and 2, *Geophys. Res. Lett*., 33, L23307, doi:10.1029/2006GL027626.

Tembe, S., D. Lockner, and T.-f. Wong (2009), Constraints on the stress state of the San Andreas Fault with analysis based on core and cuttings from San Andreas Fault Observatory at Depth (SAFOD) drilling phases 1 and 2, *J. Geophys. Res*., 114, B11401, doi:10.1029/2008JB005883.

Tembe, S., D. A. Lockner, and T.-F. Wong (2010), Effect of clay content and mineralogy on frictional sliding behavior of simulated gouges: Binary and ternary mixtures of quartz, illite, and montmorillonite, *J. Geophys. Res*., 115, B03416, doi:10.1029/2009JB006383.

Titus, S. J., C. DeMets, and B. Tikoff (2006), Thirty-five-year creep rates for the creeping segment of the San Andreas fault and the effects of the 2004 Parkfield earthquake: Constraints from alignment arrays, continuous global positioning system, and creepmeters, *Bull. Seismol. Soc. Amer., 96*, S250-S268, doi: 10.1785/0120050811.

Tocher, D. (1960), Creep on the San Andreas fault-creep rate and related measurements at Vineyard, California, *Bull. Seismol. Soc. Amer., 50*, 396–404.

Townend, J., and M. D. Zoback (2004), Regional tectonic stress near the San Andreas fault in central and southern California, *Geophys. Res. Lett*., 31, L15S11, doi:10.1029/2003GL018918.

Williams, C. F., F. V. Grubb, and S. P. Galanis Jr. (2004), Heat flow in the SAFOD pilot hole and implications for the strength of the San Andreas Fault, *Geophys. Res. Lett*. , 31 , L15S14, doi:10.1029/2003GL019352.

Wintsch, R. P., R. Christoffersen, and A. K. Kronenberg (1995), Fluid-rock reaction weakening of fault zones, *J. Geophys. Res., 100*, 13021-13032.

Zoback, M., S. Hickman, and W. Ellsworth (2010), Scientific drilling into the San Andreas Fault Zone, *Eos Trans. AGU, 91*, 197–204.

Zoback, M. D., M. L. Zoback, V. S. Mount, J. Suppe, J. P. Eaton, J. H. Healy, D. Oppenheimer, P. Reasenberg, L. Jones, C. B. Raleigh, I. G. Wong, O. Scotti, and C. Wentworth (1987), New evidence on the state of stress of the San Andreas Fault system, *Science, 238,* 1105-1111.

VITA

Clayton Gage Coble

4042 Ravencrest Ct.
Pearland TX, 77584
claycob@tamu.ed**u**

Education

M.S., Geology, Texas A&M University, College Station, TX, December 2010

B.S., Geology and Geography, Sam Houston State University, Huntsville, TX,

December 2006

Professional Experience

Texas A&M University College Station, TX
Research and Teaching Assistant August 2007 – May 2010

ConocoPhillips Houston, TX
Geology Intern June 2009 – August 2009

Honors and Awards

ConocoPhillips SPIRIT Scholarship
-Texas A&M University, 2008

Houston Geological Society Undergraduate Scholarship
-Sam Houston State University, 2006

Sam Houston Association of Geology Students Scholarship
-Sam Houston State University, 2006

Elton M. Scott Geography Scholarship
-Sam Houston State University, 2006